A&A manuscript no.
(will be inserted by hand later)

Your thesaurus codes are:
08 (08.01.2; 08.03.4; 08.06.2; 08.12.2; 08.12.3; 08.16.5)

ASTRONOMY AND ASTROPHYSICS
May 10, 2000

Probing the brown dwarf population of the Chamaeleon I star forming region *

F. Comerón[1], **R. Neuhäuser**[2], **and A. A. Kaas**[3]

[1] European Southern Observatory, Karl-Schwarzschild-Str.2, D-85748 Garching bei München, Germany
email: fcomeron@eso.org
[2] MPI Extraterrestrische Physik, Giessenbachstrasse 1, D-85740 Garching bei München, Germany
email: rne@mpe.mpg.de
[3] European Space Agency, Astrophysics Division, Keplerlaan 1, NL-2201AZ Noordwijk, The Netherlands
email: akaas@astro.estec.esa.nl

Received; accepted

Abstract. We present observations of a sample of 13 very low mass stars and brown dwarfs in the central region of the Chamaeleon I star forming cloud. The observations include slitless spectroscopy around Hα to identify new members, low resolution long-slit visible and near-infrared spectroscopy, deep ROSAT PSPC X-ray observations, and ISOCAM mid-infrared observations. Our sample adds seven new objects to those discussed by Comerón, Rieke, and Neuhäuser (1999, A&A, 343, 477) and extends the range of spectral types up to M8. We study different narrow-band indices as a tool for detecting and classifying very late-type young stellar objects. As to K-band spectra, we find that the visible features are not appropriate to yield a spectral classification more accurate than a few subclasses at best beyond M6.

None of our sources displays K-band excess emission, but four have excess at 6.7 μm suggesting that, although circumstellar disks are common around young very low mass stars, their inner regions are in general not hot enough to radiate significantly in the K band. Mid-infrared emission loosely correlates with Hα emission: sources without mid-IR excesses are always weak Hα emitters, while mid-IR excess sources have a broad range of Hα equivalent widths. X-ray emission is detected for 7 objects with spectral type M6 or later, including one bona-fide brown dwarf and three objects near the border separating stars and brown dwarfs. X-ray to bolometric luminosity ratios are typical of low mass, fully convective stars. The non-detection of X-ray emission at comparable levels from more evolved brown dwarfs suggests that X-ray activity may be restricted to early stages of brown dwarf evolution.

We discuss in detail the temperatures and luminosities of our objects based on their magnitudes and spectra, and use the derived values to estimate masses and ages according to two different sets of pre-main sequence evolutionary tracks. Both sets of models are in good agreement concerning the mass derived for our objects, showing that four of them are bona-fide brown dwarfs, six are transition objects, and three are low mass stars. Derived ages differ significantly depending on the adopted models, especially at the lowest masses. This is mainly due to the objects lying on opposite sides of the deuterium-burning main sequence depending on whether one or another set is used. Using Baraffe et al. (1998, A&A, 337, 403) models for the dating of each object in the area of our survey with mass below 1 M$_\odot$, we find that most have ages near $2\cdot10^6$ years, with a small spread around that value. However, a few objects appear to have ages near $2\cdot10^7$ years, suggesting that most, but not all, star formation in that region of Chamaeleon I may have happened almost simultaneously in a recent burst.

Comparing predictions on members of the star forming region based on K-band star counts with the number of members actually identified through Hα emission suggests that sensitive Hα surveys are very efficient in producing a complete or nearly complete magnitude-limited census of young stellar objects in Chamaeleon I. Under the assumption that our sample is complete, we derive a mass function of Chamaeleon I between 0.03 and 1 M$_\odot$ which can be approximated by a nearly flat powerlaw in logarithmic mass units, in agreement with results for other young aggregates.

Key words: Stars: pre-main sequence; low-mass, brown dwarfs; activity; circumstellar matter; formation; mass function

Send offprint requests to: F. Comerón

* Based on observations collected at the European Southern Observatory (La Silla, Chile), programs 63.L-0023 and 63.I-0546; with ISO, an ESA project with instruments funded by ESA Member States (especially the PI countries: France, Germany, the Netherlands and the United Kingdom) with the participation of ISAS and NASA; and with ROSAT, a X-ray satellite supported by the Max-Planck-Society and the German Government (BMBF/DLR).

1. Introduction

Young star forming regions within a few hundred parsecs from the Sun, like those in Orion, Taurus, Ophiuchus, Serpens, R Coronae Australis, Lupus, or Chamaeleon, have become one of the main targets for studies of the lowest mass stars and brown dwarfs. Deep surveys plus high resolution, multiwavelength observations of the faintest members of these aggregates from the ground and from space have opened up the possibility of studying in detail multiple aspects concerning their intrinsic and collective properties. These observations provide essential insights on features accompanying the earliest phases of the life of a star, such as the generation of the magnetic field, the onset of nuclear reactions at the core, the evolution of the circumstellar envelope or disk, or the late stages of accretion onto the surface. They also contain information on the processes determining the build-up of the stellar mass function or the formation of multiple systems.

An important question is to what extent the observational signatures displayed by young very low mass stars are also common to young brown dwarfs. Some basic similarities between these two classes of objects at ages of only a few million years are predicted by theoretical models, and hinted for instance by the similar properties of Hα emission (Luhman et al. 1997; Comerón et al. 1999a, hereafter CRN) or X ray emission detected from recently formed brown dwarfs (Neuhäuser & Comerón 1998, hereafter NC, Neuhäuser et al. 1999). On the other hand, the shape of the stellar mass function and the statistics of binarity in the brown dwarf domain may provide information on the relative importance of the competing processes of fragmentation and accretion at very low masses, thus constraining models on the collapse of molecular cores all the way through the formation of the compact object (Shu et al. 1987), either star or brown dwarf. An investigation of all these aspects from an observational perspective must be based on the existence of samples as large as possible, so that the different features under study can be conveniently correlated and conclusions on collective properties can be made statistically sound. This requires the use of appropriate techniques for the detection and identification of the objects of interest and, once such identifications are made, the investment of considerable amounts of observing time with a variety of highly sensitive astronomical instruments to collect multiwavelength information of each individual object.

The Chamaeleon I complex of star forming clouds and young stars (Schwartz 1991) is one of the most promising grounds for observational projects on young very low mass objects. It is nearby (160 pc; Wichmann et al. 1998, Knude & Høg 1998), the extinction is low as compared to other star forming regions (Cambrésy et al. 1997, Cambrésy 1999), and it lies at a relatively high galactic latitude, implying a moderate density of background objects. The highest concentration of members is found in the proximities of the star HD 97048. As shown by visible-light pictures, this star lies near the middle of a low extinction strip running roughly from Northeast to Southwest. Other bright members of the aggregate, like LkHα 332-17 and VW Cha, are located in this region too (Lawson et al. 1996, and references therein). A new, deep Hα objective prism and near-infrared imaging survey of a $\sim$ 100 arcmin^2 of this area, centered at $\alpha = 11^h07^m26^s$, $\delta = -77°36'50''$ (J2000.0), was presented by CRN. This survey revealed six new emission line sources, rising the number of members identified in the area to 18, most of them with M-type spectra. It also constrained the number of non-identified members and the slope of the initial mass function by means of K-band star counts.

In this paper we report on new results from a deeper survey and follow-up observations of the same area as studied in CRN, as well as a survey of an adjacent region South of that one. The available material now includes visible and near infrared imaging, near infrared low resolution spectroscopy, and space-based observations in X-rays and the thermal infrared. The study presented here greatly expands the work of CRN, both concerning to the quantity of objects discussed as to the quantity and quality of information available for most of the objects. The observational material and some details of the observations are described in Section 2. Section 3 presents a variety of results derived from these observations, concerning the visible and near infrared photometric and spectroscopic properties, as well as the X-ray and mid-infrared properties of the objects under study. The discussion in Section 4 focuses on the H-R diagram at the lowest masses and the implications concerning the evolutionary status and the mass funcion in that range. Our conclusions are summarized in Section 5.

2. Observations

2.1. Ground-based observations

The ground-based observations presented in this paper consist of:

- A deeper slitless spectroscopy survey of the area studied in CRN, for which we carried out additional observations using DFOSC at the Danish 1.5 m telescope in La Silla on 26 and 27 March 1999. We used the same instrumental setup as in the observations reported in that paper (i.e., a Gunn r filter to isolate the Hα region and reduce the bright background caused by moonlight). This made it easy to stack the new observations with the ones reported in CRN. Moreover, we improved the source detection method by implementing an automated spectrum extraction procedure, rather than relying on the visual inspection of the slitless spectroscopy frame as was done in CRN. Basically, an image of the field was used to link a reference star with its spectrum in the slitless spectroscopy frame, manually defining the spectrum extraction area. In this way, the position of the spectrum relative to the image of the object was determined. Next, sources were automatically detected in the image frame using DAOPHOT, and a spectrum was extracted for each one using the offset between the image of the star and its spectrum as defined from the reference star. A review of all the spectra obtained in this way allowed an easy and fast selection of the best targets for follow-up spectroscopy, made on the basis of Hα emission and a late spectral type as judged from the appearance of the stellar continuum feature at 6800 Å $< \lambda <$ 7100 Å. Five new late M-type emission objects were found in this way, in addition to the 17 members that had been identified in previous surveys (including the six of CRN). No attempt was made to provide a detailed classification of the other 73 spectra obtained in this field, but the vast majority clearly correspond to earlier-type, background stars.

- Slitless spectroscopy of a new area of Chamaeleon I, to the South of the one studied in CRN, carried out with the same telescope, instrument, and setup on 26-28 April 1999. The available time and observing conditions allowed us to integrate for a total of four hours on the field, thus reaching a sensitivity level similar to the one of CRN, in which the same integration time was used. Spectra were automatically extracted and examined as described above for 110 objects (the larger number with respect to the Northern field being due to the lower extinction in the Southern half of the field), nine of which displayed Hα emission. Two of them turned out to have been unidentified by previous surveys. A tenth object in the field, Cha Hα8, had most of its spectrum outside the slitless spectroscopy frame.
- Long slit low resolution spectroscopy of the objects reported by CRN, plus others discovered in a new slitless spectroscopy survey of the same area reaching to magnitudes fainter than those in CRN. Low resolution spectroscopy was carried out using EMMI, the visible imager and spectrograph at the NTT, on 17 and 18 April 1999. The grism used provided a resolving power of $\sim$ 270 over the interval 3850 Å to 10000 Å. Exposure times were adjusted according to the magnitudes of the objects and previous experience with observations of Cha Hα 1 carried out at the same telescope and with the same setup. Spectra were extracted and reduced following the same procedures used for our previous spectroscopy of Cha Hα 1, described in NC.
- Near-infrared (K band) low resolution spectroscopy of the objects reported by CRN, plus others newly discovered in the deep survey of the same area. These observations were carried out in service mode at the NTT using the infrared camera and spectrograph SOFI on 7 and 8 May 1999. The setup and data reduction process were also identical to those of our infrared observations of Cha Hα 1 in May 1998 (NC).

In addition, we make use in the present study of the JHK photometry presented by CRN, plus BVR_CI_C photometry obtained simultaneous to the slitless spectroscopy observations. The photometry was calibrated taking as a reference the magnitudes given for stars in the same field as listed by Gauvin & Strom 1992 and Lawson et al. 1996, as done in CRN, with the exception of CHXR 78NE for the reasons given in that paper. Additional medium-resolution spectroscopy of the objects described by CRN, plus two more found during the deeper slitless spectroscopy frame of the same area (Cha Hα 7 and 8), has been published in Neuhäuser & Comerón 1999. In that study, radial velocities were derived and found to be consistent with membership in the star forming region for all the studied objects. Moreover, all of them were found to show lithium absorption in their spectra, as expected from newly formed very low mass objects.

2.2. ROSAT observations

We have merged the data of two ROSAT PSPC pointed observations (31 ks by PI H. Zinnecker plus 5 ks by PI E. Feigelson) centered both on the Cha I dark cloud (see NC). Then, we have performed local and map maximum likelihood source detection – in principle very similar to what we explained and used in NC, CRN, and Neuhäuser et al. 1999. For the detection of faint sources in the PSF wings of much brighter nearby X-ray sources, we have modified the MIDAS/EXSAS detection proceedure. Originally, a preliminary (local) source detection is done first. Then, photons from detected source are removed from the background image. Then, another (map) source detection is done. Finally, the local and map sources are merged to obtain the final source list. In the revised proceedure, we do these steps in three consecutive iterations and we also scale the numbers of photons to be removed by the profile of the PSF of the detected sources. This two modifications allow us to also detect very faint sources near bright sources, e.g. Cha Hα5. A detailed description of the results is given in Section 3.4.

2.3. ISOCAM observations

The ISOCAM data are taken from a survey of Cha I in the two broad band filters LW2 (5 - 8.5 μm) and LW3 (12 - 18 μm), described by Nordh et al. (1996), Olofsson et al. (1998) and Persi et al. (2000). The region of interest in this study was covered in the $18' \times 21'$ field named "Cha I SE", observed in raster mode with $3''$/pix resolution and 0.28 seconds integration, staying a total of 15 seconds per sky position. In order to avoid saturation by bright infrared sources in the field, this lowered sensitivity, compared to

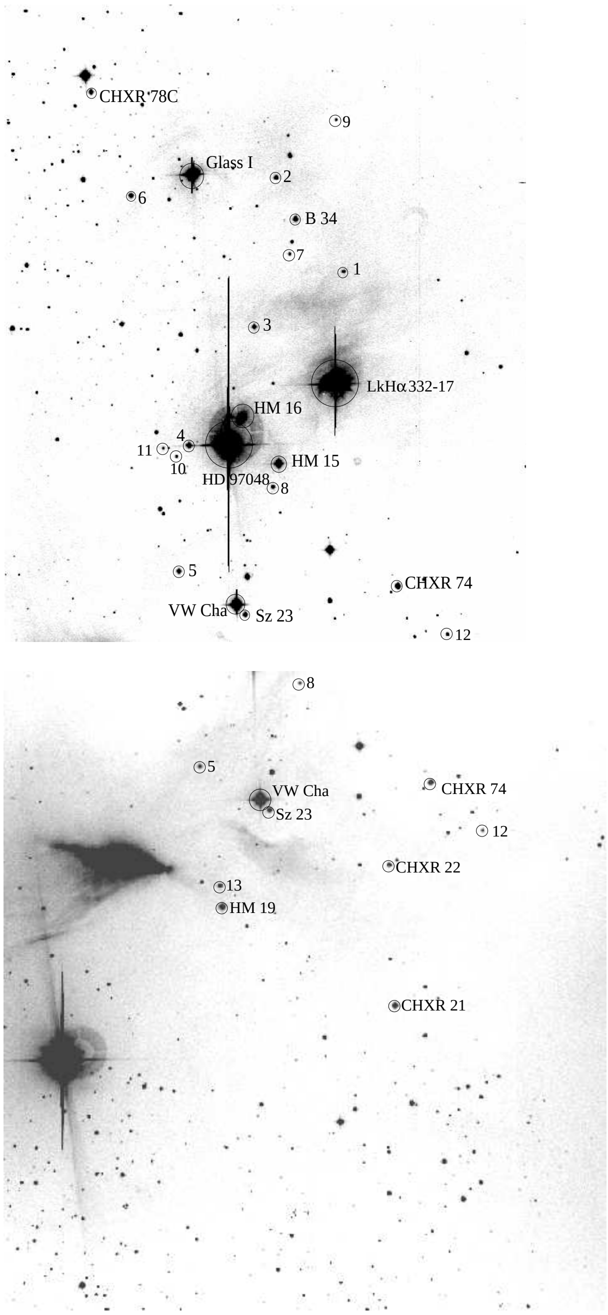

Fig. 1. Finding charts for the central region of Chamaeleon I (top) and the overlapping region South of it (bottom). All the members identified in the present and previous surveys are marked. Both images were taken with DFOSC at the 1.5 Danish telescope in La Silla, and have a field of wiev of $13' \times 13'$. North is at the top and East to the left. The top image was obtained through the I_C filter, and the bottom one through the R_C filter.

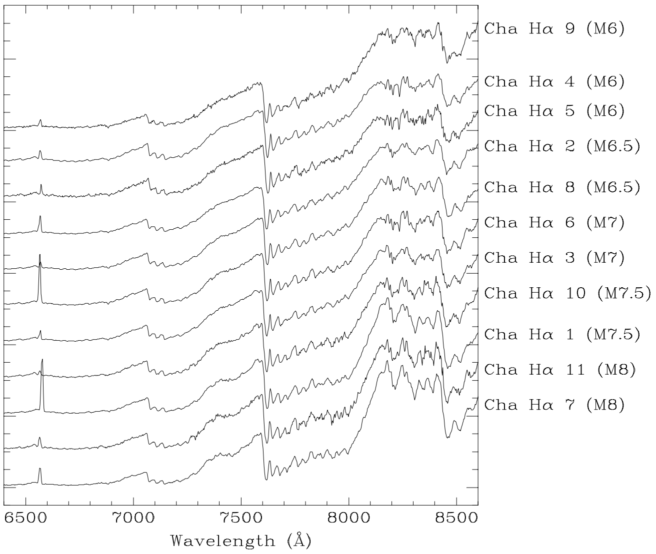

Fig. 2. Spectra of objects Cha Hα 1 to 11 at visible wavelengths, ordered by increasing spectral subtype.

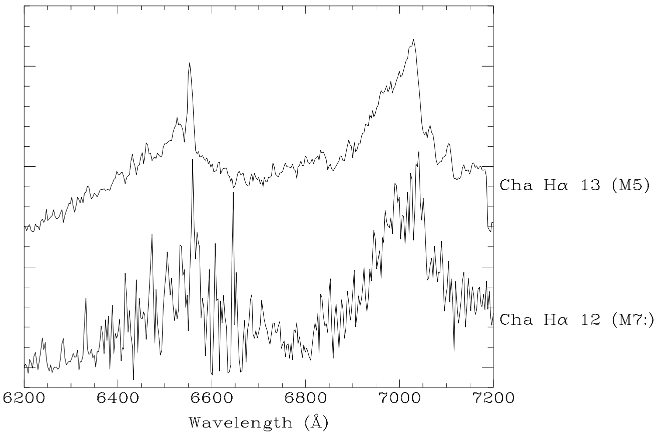

Fig. 3. Spectra of objects Cha Hα 12 and 13 in the Hα region.

the nominal set-up, was used. Data reduction was performed as described in the above references.

3. Results

3.1. New late type members and their visible spectra

The purpose of the slitless spectroscopy surveys is the identification of new, faint late type Chamaeleon I members through their Hα emission. Although Hα emission is not unique to young low mass objects, the confirmation that objects detected in this way are indeed young can be carried out with follow-up spectroscopy (CRN, Neuhäuser & Comerón 1999). The slitless spectroscopy of Chamaeleon I obtained by CRN demonstrated that lightly embedded, young brown dwarf candidates in nearby star forming aggregates are within the reach of small-sized telescopes with a modest investment of observing time.

New observations carried out using this approach have allowed us to increase the number of identified Hα emitting objects with a late M spectrum in the central region of

Chamaeleon I to 13, as compared to the 6 initially identified by CRN. Moreover, high S/N spectra covering the entire visible range (as opposed to a narrow band of $\sim$ 1000 Å around Hα of the lower S/N spectra presented by CRN) and K-band spectra for 11 of these objects are now available, including the 6 new Hα emitters studied by CRN. For the other 2, only lower S/N spectra in the 6200 Å-7200 Å range are available so far. For the 6 Hα emitters discussed by CRN and two of the newly discovered objects, medium-resolution spectroscopy has also been obtained and discussed separately (Neuhäuser & Comerón 1999).

Figure 1 contains finding charts with all the objects discussed in this paper, plus other brighter members of the aggregate that had been previously identified by other authors. The visible spectra of the objects observed with long-slit spectroscopy are displayed in Figure 2, and the Hα-region spectra of the two additional objects South of the main surveyed area are displayed in Figure 3. Table 1 lists the positions and photometry, when available, of all the objects, as well as their spectral types.

We have classified the objects for which we have the full visible spectra following the criteria described in detail by CRN for the classification of Cha Hα 1, i.e. using both the general appearance of the spectrum to compare it to a sequence of field late M dwarfs, as well as a variety of flux ratios proposed by different authors to produce a quantitative classification of M dwarfs. The spectral classifications provided in Figure 2 and in Table 1 are obtained by comparing the individual spectra to the sequence defined by Kirkpatrick et al. 1991 for field M dwarfs. Since these classifications are in general based on spectra of much better quality than those used by CRN (with the only exception of Cha Hα 1), the spectral types given in Figure 2 and Table 1 differ slightly in some cases from the ones attributed in that work. We estimate the accuracy of the spectral types derived here to be ±0.5 subtypes. Adopting these classifications as the reference ones allows us to study the behaviour of the different flux ratios in very young late-type objects, which is an important issue in deciding on both their adequacy for narrow-band imaging surveys, and their ability to discriminate between young and evolved M dwarfs.

A set of such ratios was proposed by Kirkpatrick et al. 1991 to measure the strenghts of a number of temperature- and gravity-sensitive spectral features over the range 6900 Å- 8600 Å. In general, these ratios present monotonic trends for dwarfs down to a spectral type M5-M7, and they reverse the behaviour for the latest spectral types. For ratio A, measuring the strength of the CaH feature centered at 6975 Å, our objects display a nearly uniform value of 1.34, with a scatter of less than 0.03, which is less than the typical scatter for field dwarfs. The average values that we find are similar to those of field dwarfs of types around M4.5 or later than M7. At the spectral type M6 our ratio A is below that of field dwarfs by $\sim$ 0.1, but well above that of giants. For ratio B, measuring the strength of the TiI feature near 7358 Å, we find typically values between 1.06 and 1.10, well within the range of field dwarfs between M4 and M7. Two of our objects, Cha Hα 9 (type M6) and Cha Hα 7 (M8) display somewhat higher, more giant-like values of 1.14, but the difference with field dwarfs is still small. Similarly, for ratio D measuring the CaII feature at 8542 Å we find values of 1.05-1.10, near the minimum of the values measured in field dwarfs which occurs at M5-M6. In summary, our objects are dwarf-like concerning the behaviour of ratios A, B, and D, and the fact that they lie in the range where the monotonic trends of these ratios with temperature break down makes them of little use in classifying our objects or discriminating them from field dwarfs. The similarity between the values found for our objects and those typical of field stars suggests that the veiling of the spectral features of our young objects is small at most.

A more interesting behaviour concerning Kirkpatrick et al.'s ratios is found in ratio C, which measures the strength of the NaI feature around 8190 Å. This line, and to a lesser extent the NaI line at 2.207 μm as well (Luhman & Rieke 1998), is a sensitive surface gravity indicator, able to discriminate between evolved and field dwarfs. Our results, yielding a value of the ratio between 0.8 and 1.0 for our objects, not only confirm that it is much smaller than for dwarfs (for which measured values are above 1.2 at M6), but also show that it is clearly below the ratio measured for giants as well, at least down to spectral type M5, in which ratio C is around 1.05. Ratio C is thus a very useful tool for confirming the membership of late M-type objects in star forming regions.

Concerning temperature indicators for very late-type M dwarfs, Kirkpatrick et al. 1995 have proposed the use of an index measuring the strength of the VO feature around 7445 Å as the most suitable one for spectral classification at spectral types M7 or later. We find indeed a good correlation between spectral type and VO index for our objects as well, as illustrated by Figure 4. We only find a slightly smaller VO index for a given spectral subtype when comparing the values given by Kirkpatrick et al. 1995, which may be due to remaining surface gravity effects, but the possible offset of VO-based spectral subtypes between field dwarfs and very young M-type objects does not seem to exceed 0.5 spectral subclasses.

Given the usefulness of slitless spectra including only a narrow band centered at Hα for the identification of new candidate members of star forming regions, it is interesting to check the suitability of indices defined in this region to produce a preliminary classification of the objects so found. Two useful indices in this region, denoted as R_3/R_2 and R_4/R_7, have been defined by Prosser et al. 1991 and used by CRN to classify the objects in their survey. We have calculated these indices for the 11 objects for which we have high quality visible spectra, and have found that the R_4/R_7 index (which measures the depth of the TiO bandhead at 7053 Å) continues to be well cor-

Table 1. Positions, photometry, and spectral types of faint late-type Chamaeleon I members

Name	α (2000)	δ (2000)	B	V	R_C	I_C	J	H	K	Sp. type	EW(Hα) (Å)
Cha Hα 1	11:07:17.0	-77:35:54	22.8:	21.0	18.7	16.17	13.55	12.78	12.28	M7.5	99
Cha Hα 2	11:07:43.0	-77:33:59	21.9:	19.8	17.60	15.08	12.59	11.43	11.15	M6.5	32
Cha Hα 3	11:07:52.9	-77:36:56	21.5	19.51	17.38	14.89	12.46	11.64	11.11	M7	13
Cha Hα 4	11:08:19.6	-77:39:17	20.5	18.52	16.70	14.34	12.20	11.42	11.04	M6	11
Cha Hα 5	11:08:25.6	-77:41:46	21.3	19.18	17.14	14.68	12.14	11.21	10.76	M6	11
Cha Hα 6	11:08:40.2	-77:34:17	21.7	19.75	17.60	15.13	12.43	11.61	11.09	M7	76
Cha Hα 7	11:07:38.4	-77:35:30	23.7::	22.2:	19.5	16.86	13.89	13.00	12.51	M8	45
Cha Hα 8	11:07:47.8	-77:40:08	22.2:	20.1	17.96	15.47				M6.5	9
Cha Hα 9	11:07:19.2	-77:32:52	>23.7	23.1:	20.1	17.34	13.92	12.59	11.82	M6	16
Cha Hα 10	11:08:25.6	-77:39:30	22.6:	21.6	19.4	16.90	14.41	13.68	13.27	M7.5	9
Cha Hα 11	11:08:30.8	-77:39:19	23.3::	21.9	19.9	17.35	14.72	13.98	13.57	M8	23
Cha Hα 12	11:06:37.5	-77:43:07	>21.3	20.6	18.3	15.58				M7:	20:
Cha Hα 13	11:08:18.4	-77:44:12	20.4	18.46	16.58	14.09				M5	11

Magnitudes indicated with two decimal are those having accuracies of 0.05 or better; a colon indicates an uncertainty greater than 0.2, and two colons, greater than 0.5.

related with the spectral index well beyond the M5.5 type originally considered by Prosser et al. 1991, as shown by the middle panel of Figure 4. Our classification of Cha Hα 12 and 13 given in Table 1 and Figure 3 is based on this index. Judging from the appearance of L-type spectra (Kirkpatrick et al. 1999), the correlation may extend down to about L1. A poorer correlation is found for the ratio R_3/R_2, which may be largely due to inaccuracies in the artificial subtraction of the Hα line present in the R_2 band. The need to remove the Hα emission, and the subsequent errors and biases derived from the subjective estimate of the continuum level, discourage the use of this index for strong Hα emitting objects like the ones discussed here.

We finally considered the pseudocontinuum indices proposed by Martín et al. 1996 for the classification of young brown dwarfs, with the exception of indices PC4 and PC5 which require measurements at wavelengths beyond the interval covered by our spectra. In general we find a poor correlation of the three indices considered (PC1, PC2, and PC3) with the spectral type, and values systematically higher than those found by Martín et al. 1996. Unlike the indices described in the previous paragraphs, these pseudocontinuum ratios involve fluxes measured at wavelengths typically 500 Å apart, and extinction effects, even for relatively lightly embedded sources like ours, can be noticeable. The scatter and systematic effects that we see in our data are consitent with such an explanation. Since a proper correction for reddening is not straightforward (see Section 3.3), we consider that spectral classification based on pseudocontinuum indices is not adequate for objects whose foreground extinction may be important, such as those discussed here.

3.2. Near-infrared spectra

The availability of both visible and near-infrared spectra for a sample of 11 Chamaeleon I members of types M6-M8 offers a good opportunity to study the correspondence between both, and therefore the possibility of establishing a near-infrared spectral sequence for very young late-type objects. Such a spectral sequence should be of great use for the study of other star forming regions, whose members are too heavily obscured for spectroscopy in the visible and where the K band is the only accessible domain for spectral classification. Spectral sequences for late M dwarfs in the near infrared have been published by Jones et al. 1994 (see also Williams et al. 1995 for references on earlier work), and detailed comparisons between atmosphere models and observed spectral features in the infrared with the purpose of establishing a temperature scale have been carried out by Leggett et al. 1996 and Jones et al. 1996. These and other works have been based on field M dwarfs, whose surface gravity exceeds by more than one order of magnitude that typical of brown dwarfs in star forming regions. Therefore, their results may not be directly applicable to very young objects such as the ones studied here. In a different approach, Luhman & Rieke 1998 used visible spectra of a sample of late-type members of the L1495E cloud, selected by their Hα or X-ray emission, to empirically calibrate the M spectral sequence of very young objects in the infrared. They performed a careful analysis to quantify the degree of veiling in the K band, which can affect spectral features at that wavelength. The latest spectral type included in their analysis, M6, just falls short of probing the brown dwarf region. More recently, Luhman 1999 have extended the comparison between visible and infrared spectra in a star forming region to IC 348. Although three likely brown dwarfs are included in their sample with spectral types as

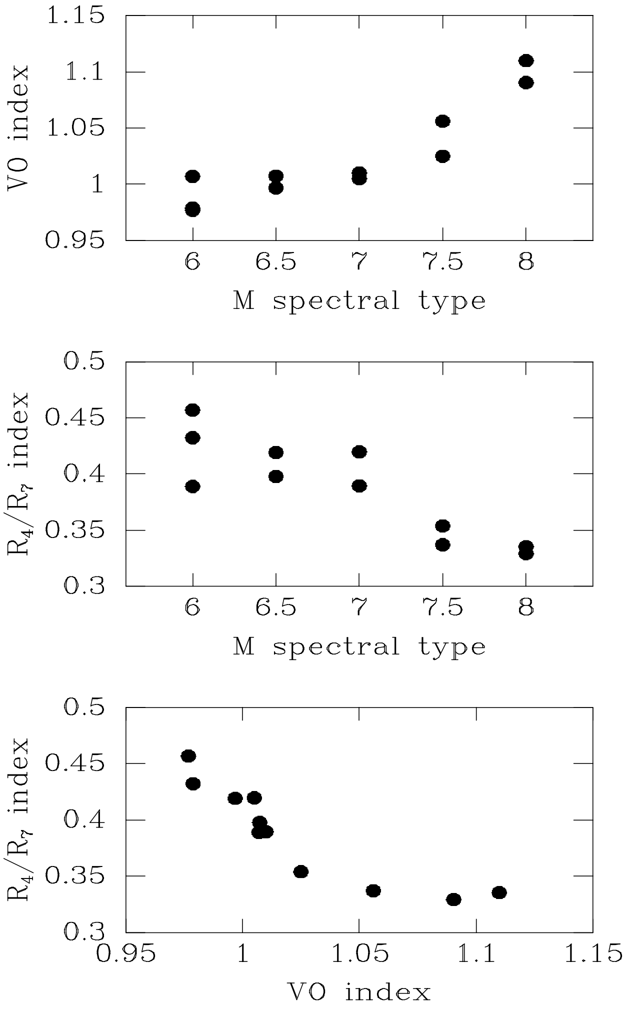

Fig. 4. Evolution of the VO and R_4/R_7 indices (see text) versus spectral type and versus each other. Both indices provide useful quantitative criteria for spectral classification, although the VO index is clearly preferrable whenever both are available.

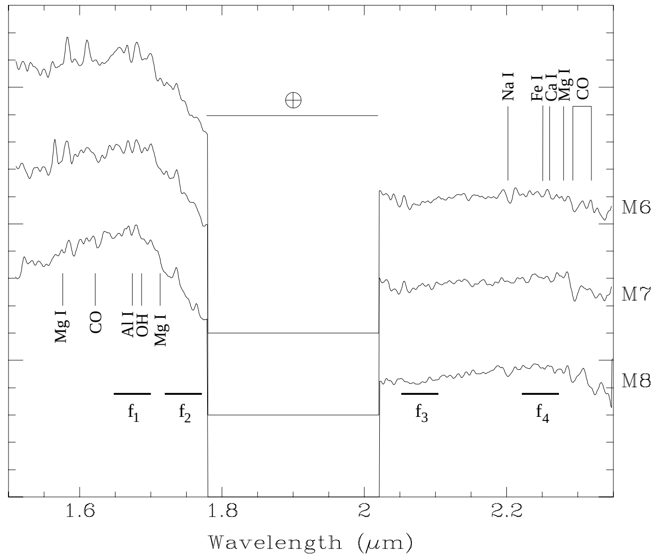

Fig. 5. Infrared spectra in the long wavelength portion of the H band and in the K band. The spectrum marked as M6 is the sum of the spectra of Cha Hα 4, 5, and 10; M7 is the sum of Cha Hα 2, 3, 6, and 8; and M8 is the sum of Cha Hα 1, 7, 10, and 11. The spectra have been ratioed by that of a late O-type star observed at a similar airmass to correct for telluric features, and multiplied by a blackbody spectrum at 35,000 K to obtain a relative flux calibration. The main features that appear in H and K band spectra of late M dwarfs are indicated. Also indicated are the positions of the narrow bands in which the fluxes f_1, f_2, f_3, and f_4 proposed in Section 3.2 are measured. The blank interval centered near $\lambda = 1.9$ μm and marked as $\oplus$ is due to telluric absorption.

late as M8, they were too faint for infrared spectra to be obtained. Some possible and bona-fide brown dwarfs have been observed spectroscopically in the ρ Ophiuchi cloud (Williams et al. 1995; Luhman & Rieke 1999; Wilking et al. 1999), but spectra both in the infrared and in the visible have not been obtained yet for any of these objects. Our sample of types later than M6 is thus well suited to extend the calibration of near-infrared spectra into the brown dwarf domain.

Unfortunately, the signal-to-noise ratios for some our faintest objects is insufficient for spectral classification purposes. However, the fact of having in our sample many objects within a narrow range of spectral types allows us to produce averaged spectra with higher signal-to-noise ratio by combining those of all the objects with similar spectral types. In this way, we have produced representative near-infrared spectra for M6 objects by combining those of Cha Hα 4, 5, and 9; for M7 objects, by combining those of Cha α 2, 8, 3, and 6 (i.e., individual types M6.5 and M7); and for M8 objects, by combining those of Cha Hα 1, 10, 8, and 11 (i.e., individual types M7.5 and M8). In this latter group we have also included the spectrum of Cha Hα 1 presented and discussed by NC. Given the low extinction at near-infrared wavelengths in the direction of all those objects and their lack of near-infrared excesses as derived from the available BVR_CI_CJHK photometry (see Section 3.3), the reduced spectra have been directly combined without any further corrections. The combined spectra are shown in Figure 5. The positions of the main spectral features expected in both the H and the K band are marked. However, the spectra are expected to be very nearly featureless in the H band, according to the spectral sequence in that domain presented by Meyer et al. 1998: the strongest feature observed in their latest-type M dwarf, GL 725A (type M3V) is the AlI (1.6742 μm) line with an equivalent width of 3.5 Å, near the detection limit of our composite spectra.

Although Luhman & Rieke 1998 identified useful correlations between the spectral type and the strength of some features, such correlations break down at the late spectral types under consideration here. This was already

Table 2. Equivalent widths (in Å) of the main features observed in our K-band spectra.

spectral type	NaI (2.21 μm)	CaI (2.26 μm)	CO (2.29 μm)
M6	7 ± 2	3 ± 1	9 ± 2
M7	3 ± 1	4 ± 1	16 ± 3
M8	6 ± 2	1 ± 1	13 ± 3

pointed out for field dwarfs by Luhman & Rieke 1998, and is confirmed by our measurements of the most prominent features observed in the K band that we list in Table 2, in which no clear correlation with spectral type is apparent for any of them. Spectral classification based on these narrow features, at least at the resolution and signal-to-noise ratio that can be normally attained with current instrumentation, does not seem to be feasible to an accuracy level of a few spectral subtypes.

An alternative way suggested by Wilking et al. 1999 in based on the use of the broad H_2O bands which appear at the limits of the atmospheric K window. Wilking et al. defined a reddening-free Q index based on the ratios of fluxes in narrow wavelength intervals, some of which include the wings of the H_2O absorption. One of the intervals runs from 2.4 to 2.5 μm, a region in which our spectra are poorly observed due to the rapid increase of the atmospheric background emission (Wilking et al. used spectra obtained with the IRTF from Mauna Kea, a site with much better average near-infrared conditions than La Silla). Therefore, our data do not allow us to obtain reliable values of the Q index as defined by Wilking et al. 1999. We can nevertheless define another reddening-free index, $I_{\rm H_2O}$, measuring the depth of the wings of the water band centered near 1.9 μm. To do this, we define four bands of 0.05 μm width each centered at the wavelengths of 1.675μm, 1.750μm, 2.075μm, and 2.250μm, calling f_1, f_2, f_3, and f_4 to the respective fluxes measured in each of these bands. We assume that the extinction law is the same as derived by Rieke & Lebofsky 1985, which we approximate as $A_\lambda \propto \lambda^{-1.47}$ over the H and K bands as done Wilking et al. 1999. In this way, our $I_{\rm H_2O}$ is defined as

$$I_{\rm H_2O} = \frac{f_1}{f_2}\left(\frac{f_4}{f_3}\right)^{0.76} \tag{1}$$

When $I_{\rm H_2O}$ is calculated for our objects, we obtain values between 1.19 and 1.48 without any apparent correlation with the spectral subtype. This may be due to the narrow range of subtypes represented by our spectra, in agreement with the accuracy of ±1.5 subclasses estimated by Wilking et al. 1999 for their Q index. However, it may also be due to saturation effects, as suggested by the comparison among infrared spectra of the latest field M dwarfs and L dwarfs (Kirkpatrick et al. 1999). Luhman & Rieke 1999 hinted that such effects may be visible in very young M-type objects at spectral types as early as M6. Although our data do not allow to discern between these two possibilities, it seems clear that no accurate spectral classification based on near infrared spectra like the ones presented here is possible.

3.3. Extinction and near infrared excess

To estimate the extinction in the direction to each of our sources, we use the accurate spectral types available for most of them together with empirical calibrations of intrinsic colour vs. spectral type, and then compare the intrinsic and observed colours to obtain the reddening. This was already done by CRN using the $(I_C - H)$ colour index, or $(V - I_C)$ when the latter was not available. The intrinsic colour indices adopted in that work were those compiled by Kenyon & Hartmann 1995, based on field objects and extending down to spectral type M6. Such a choice has the double inconvenient of being based on objects of systematically higher surface gravity than those considered here, and of requiring a rather large extrapolation to reach to M8. For the present work, we have preferred instead to use an intrinsic colour index vs. spectral type relationship based on the observations of very low mass stars and brown dwarfs in the Pleiades published by Zapatero-Osorio et al. 1997. This calibration has the advantage of including later-type spectra than those tabulated by Kenyon & Hartmann 1995, and of being based on objects that, although older than ours, should have physical characteristics closer to them than field M dwarfs. As seen from table 1 of Zapatero-Osorio et al. 1997, the $(R_C - I_C)$ index is the one showing the most regular behaviour with spectral type, and therefore we have used it for our calculations, as moreover it is available for all our sources[1]. The age difference between the members of the Pleiades (ages $\sim 10^8$ years) and of Chamaeleon I (ages $< 10^7$ years) may be expected to produce somewhat bluer (i.e., giant-like) $(R_C - I_C)_0$ indices for our objects at a given spectral type. The difference between the indices for Pleiades (Zapatero-Osorio et al. 1997) and giants (Fluks 1998) is approximately 0.40 mag over the interval M6-M8. Given the rather dwarf-like appearance of our spectra, and lacking more quantitative criteria for the determination of the correction to be applied to the colours measured by Zapatero-Osorio et al. 1997, we have decided rather arbitrarily to assume intrinsic $(R_C - I_C)_0$ colours for our objects bluer by 0.10 mag than those listed in that work, of which 0.03 mag would correspond to the foreground reddening in the direction of the Pleiades (Crawford & Perry 1976). The values observed within a given spectral type have then been averaged, and these averages have

[1] $(V - I_C)$, having a larger baseline, may be more suitable to derive the extinction, but the faintness of many of our objects in V and the subsequent lesser photometric accuracy discourages its use.

Table 3. Adopted intrinsic colour indices $(R_C - I_C)_0$, $(H - K)_0$

spectral type	$(R_C - I_C)_0$	$(H - K)_0$
M6	2.20	0.30
M6.5	2.30	0.35
M7	2.40	0.40
M7.5	2.50	0.45
M8	2.60	0.50

then been fitted as a linear function of the spectral type. The adopted colour index vs. spectral type calibration is listed in Table 3, and we estimate it to be accurate to $\simeq 0.10$ mag.

We calculate the extinctions in the I_C band as

$$A_I = 1.812[(R_C - I_C) - (R_C - I_C)_0] \quad (2)$$

where $(R_C - I_C)$ is the observed spectral index. The coefficient 1.812 comes from the extinction law of Rieke & Lebofsky 1985. The actual value for Chamaeleon I may be somewhat different (Whittet et al. 1987), as sometimes observed in star forming regions. However, given that deviations from the standard extinction law tend to decrease towards longer wavelengths and that the extinctions towards our objects are small, especially in the I_C band in which we will base our luminosity estimates, we are confident that the possible errors introduced by our choice of the extinction law are not significant.

K-band infrared excesses are usually an indicator of the presence of circumstellar material in the proximity of a star (e.g. Meyer et al. 1997). For some of our objects, the presence of circumstellar material can be much better assessed or constrained by its emission at the longer wavelengths imaged by ISO (see Section 3.5). However, K-band excess is a sign of caution in interpreting the near-infrared spectra, as it may indicate a significant amount of veiling of the spectral features in that region (Luhman & Rieke 1998). It is thus important to check for its possible presence in our objects.

Near-infrared excesses can be expressed as

$$\Delta(H - K) = (H - K) - (H - K)_0 - 0.38A_I \quad (3)$$

where $(H-K)$ and $(H-K)_0$ are respectively the observed and intrinsic colour indices. For the $(H - K)_0$ colour indices we have directly averaged and fitted the $(H - K)$ values measured by Zapatero-Osorio et al. 1997, with no corrections in this case due to the insignificant reddening in $(H - K)$ towards the Pleiades and the small difference (0.05 mag or less) between those averaged values and the ones determined for giants between M6 and M8 (Fluks 1998). The adopted $(H - K)_0$ colours are listed in Table 3.

Table 4 lists the extinction and near-infrared excess derived for our sources. It should be noted that these quantities (actually, in the J band in the case of the extinction)

Table 4. Extinctions and near-infrared excesses

spectral type	A_I	$\Delta(H - K)$
Cha Hα 1	0.11	0.01
Cha Hα 2	0.40	-0.22
Cha Hα 3	0.16	0.07
Cha Hα 4	0.29	-0.03
Cha Hα 5	0.47	-0.03
Cha Hα 6	0.13	0.07
Cha Hα 7	0.14	-0.06
Cha Hα 8	0.34	
Cha Hα 9	0.76	0.18
Cha Hα 10	0.05	-0.06
Cha Hα 11	0*	-0.09
Cha Hα 12	0.5:	
Cha Hα 13	0.89	

*: The adopted $(R_C - I_C)$, $(R_C - I_C)_0$ would give $A_I = -0.11$ for this object. We have assumed $A_I = 0$.

were already derived for objects 1 to 6 by CRN. The small discrepancies between the present values and those found in that work are due to the somewhat different procedure used to calculate them, as remarked above, as well as to the slightly different spectral classifications in some instances as a consequence of the much better spectra available now. It can be seen that none of our objects displays a significant $\Delta(H - K)$, and the values of Cha Hα 2 and Cha Hα 9 can be due to the combination of photometric errors and deviations from the intrinsic colours and extinction law assumed here. This confirms that the correlation between strong Hα emission and K-band excess emission that is commonly observed for brighter objects does not apply anymore at the very low luminosities that we are dealing with here, probably due to the insufficient temperature of the inner parts of the circumstellar disk. This will be discussed in more detail in Section 3.5. However, it is intriguing that K-band excess does seem to exist in other very low mass objects observed in other star forming regions, as discussed by CRN, who identified 2-3 faint sources with K-band excess in the near-infrared survey of the area discussed here. In addition, Oasa et al. 1999 have reported the existence of some very faint objects, possibly brown dwarfs, with apparent K-band excess in the Nothern part of the Chamaeleon I complex.

3.4. Results on X-ray emission.

The improvements in sensitivity near bright X-ray sources provided by our upgraded EXSAS source detection routine, as outlined in Section 2.2, enables us now to obtain detections for Cha Hα 4 and 5, which are located very close to the bright X-ray sources HD 97048 and VW

Table 5. X-ray data of Cha Hα 1 to 13

Object	off-set [arcsec]	off-axis [arcmin]	Exp. [ks]	ML	X-ray counts	Hardness ratios HR 1	HR 2	log L_X [erg/s]	log L_X/L_{bol}
Cha Hα 1	3.8	5.0	37.8	33.6	31.7 ± 7.8	≥ -0.33	0.15 ± 0.22	28.41 ± 0.10	-3.21
Cha Hα 2	(n.r.)	5.5	37.8	not resolved from nearby bright X-ray source CHXR 26 (*)					
Cha Hα 3	16.8	7.1	37.5	11.3	12.1 ± 4.2	≥ -0.60	0.05 ± 0.34	28.00 ± 0.13	-4.12
Cha Hα 4	15.9	9.7	37.0	28.4	21.0 ± 7.9	0.78 ± 0.60	0.53 ± 0.27	28.25 ± 0.13	-4.08
Cha Hα 5	14.0	11.7	35.1	16.2	29.1 ± 8.2	0.55 ± 0.84	0.29 ± 0.56	28.41 ± 0.11	-3.86
Cha Hα 6	10.3	8.6	31.8	7.2	9.4 ± 5.3	≥ -0.66	-0.08 ± 0.41	27.96 ± 0.20	-4.05
Cha Hα 7	(n.r.)	5.7	37.8	not resolved from nearby bright X-ray source B 34 (*)					
Cha Hα 8	(n.r.)	9.1	37.1	not resolved from nearby bright X-ray source HM 15 (*)					
Cha Hα 9	(n.d.)	4.1	35.8	(n.d.)	≤ 12.9	(n.d.)	(n.d.)	≤ 28.05	≤ -3.27
Cha Hα 10	(n.r.)	10.1	37.0	not resolved from nearby X-ray source Cha Hα 4					
Cha Hα 11	(n.r.)	10.2	37.0	not resolved from nearby X-ray source Cha Hα 4					
Cha Hα 12	1.2	10.3	36.5	26.8	24.8 ± 7.6	0.79 ± 0.64	0.74 ± 0.22	28.32 ± 0.11	-3.66
Cha Hα 13	13.9	13.4	35.2	98.7	81.1 ± 11.7	0.83 ± 0.16	0.20 ± 0.13	28.85 ± 0.06	-3.76

Remarks: Off-set is distance between X-ray and optical position (n.r. for not resolved, n.d. for not detected). Off-axis is distance between the center of the X-ray pointed observation and the X-ray source position. ML is maximum likelihood for existence of X-ray source (ML=5 is $\sim 3\,\sigma$). X-ray luminosities L_X at 160 pc distance for absorbed one-temperature (1 keV) Raymond-Smith X-ray spectra (see text for details).
(*) Unresolved X-ray source is elongated towards the Cha Hα object.

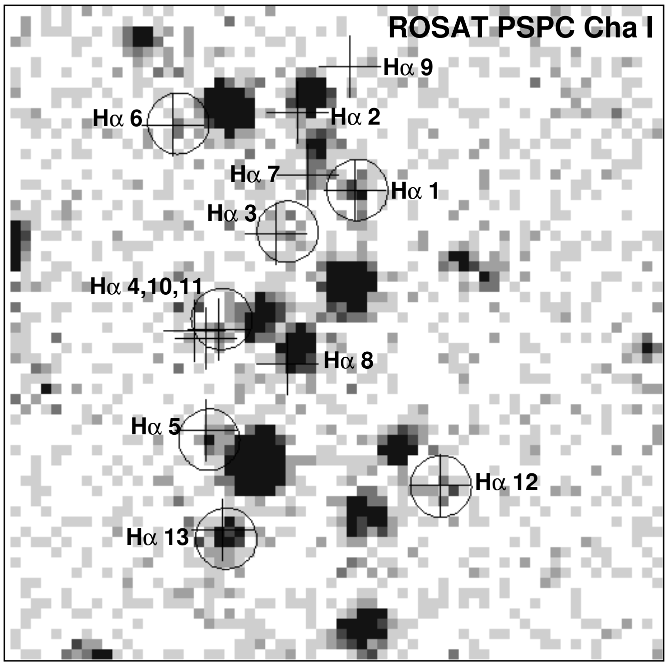

Fig. 6. ROSAT PSPC image of central part of Cha I dark cloud with the objects Cha Hα 1 to 13 marked as crosses. X-ray sources identified with any of those objects are marked by circles (centered on the X-ray positions). The remaining bright X-ray sources visible on this image are other young stars in Cha I. Cha Hα 1, 3, 4, 5, 6, 12, and 13 are detected, Cha Hα 2, 7, 8, 10, and 11 are unresolved, and Cha Hα 9 is clearly undetected.

Cha, respectively [2]. On the other hand, the X-ray emission of Cha Hα 1, first reported in NC, has been recently confirmed by ASCA observations (Tsuboi, Koyama, and Neuhäuser, in prep.). Still, Cha Hα 2, 7, 8, 10, and 11 cannot be resolved from other nearby X-ray sources. However, as far as Cha Hα 2, 7, and 8 are concerned, they are located next to bright X-ray sources that are elongated towards them, and therefore they are probably also faint X-ray sources. They should be detectable and resolvable with Chandra. The X-ray source identified as Cha Hα 4 is located close to Cha Hα 10 and 11 too, but Cha Hα 4 is much closer to the X-ray source. We also present new detections of Cha Hα 12 and 13. All X-ray data are listed in Table 5. The ROSAT PSPC image is shown in Figure 6. Cha Hα 9 is undetected, and we present upper limits.

For converting the observed count rate (or an upper limit) to an X-ray luminosity, we assume that the objects emit one-temperature Raymond-Smith X-ray spectra, like low-mass pre-main sequence T Tauri stars. We assume 1 keV as the energy of the emitting plasma. This is justified, because the late-type young T Tauri stars studied by Neuhäuser et al. (1995) in Taurus are observed to emit such spectra, and they should be similar coronal sources as our low-mass objects in Cha I. For the individual absorbing column density, we can use the A_I values listed in Table 4. Those values range from $A_I = 0.05$ to 0.89 mag, which corresponds to $\log(N_{\rm H}/{\rm cm}^{-2}) \simeq 20.2$ to 21.5. As seen in Figure 3 of Neuhäuser et al. 1995, the energy conversion factor is very flat in this parameter range, so that we can use 10^{11} cts cm^{-2} erg^{-1} for all objects. Within their 1-σ error bars, the values are not different from those listed before in NC, CRN, and Neuhäuser et al. 1999. For estimating the X-ray to bolometric luminosity ratio, we

[2] Note that we used and listed a slightly wrong position for Cha Hα 5 in NC, CRN, and Neuhäuser et al. 1999, but correct in Neuhäuser & Comerón 1999.

use the $L_{\rm bol}$ values listed in Table 6, which have been revised as compared to CRN (see Section 4.1). Hence, the $L_{\rm X}/L_{\rm bol}$ values change accordingly compared to NC, CRN, and Neuhäuser et al. 1999.

The X-ray detected young M6 to M8 dwarfs in Cha I all have X-ray luminosities of $\log L_{\rm X}({\rm erg\ s}^{-1}) \simeq 28$, which is confirmed to be the typical X-ray luminosity of young late M-type T Tauri stars and brown dwarfs (see NC, CRN, and Neuhäuser et al. 1999). Cha Hα 13 with the earliest spectral type (M5) is brighter in X-rays than all other objects studied here. The X-ray to bolometric luminosity ratio ranges from $\sim 10^{-3}$ to $\sim 10^{-4}$, similar to normal late M-type stars.

In Neuhäuser et al. 1999, only one additional bona-fide brown dwarf (ρ Oph GY 202) and only four candidate brown dwarfs (V410 x-ray 3, V410 Anon 13, MHO-4, and MHO-5) were detected as faint X-ray sources. Like the Cha Hα objects studied here, they are all located in star forming regions, i.e. have similar ages, $\sim$ 1 Myr. More recently, X-ray detections with Chandra of at least two brown dwarf candidates in the Trapezium cluster have been reported by Hillenbrandt 2000. Neither the intermediate age Pleiades brown dwarfs ($\sim 10^8$ yrs at $\sim$ 125 pc) nor the old but nearby field brown dwarfs have been detected as X-ray sources, despite of some very deep pointed observations. Hence, many of them are fainter than young brown dwarfs in terms of X-ray luminosity $L_{\rm X}$. Because the Pleiades and field brown dwarfs are older than the brown dwarfs in star forming regions, they are also fainter in $L_{\rm bol}$. The upper limits to their $L_{\rm X}/L_{\rm bol}$ ratios (see Neuhäuser et al. 1999) are only rarely in the range obtained here for Cha I (see Table 5). More sensitive X-ray telescopes (e.g. XMM) are needed to test whether or not brown dwarfs at the age of the Pleiades or older emit X-rays. The recent detection by Chandra of the bona-fide brown dwarf LP944-20 during a flare (G. Basri, priv. comm.) suggests that indeed increased sensitivity may reveal at least episodic X-ray activity from evolved brown dwarfs. Nevertheless, the level of possible quiescent X-ray emission of field brown dwarfs remains an open question.

If confirmed that only young brown dwarfs emit quiescent X-rays, a number of explanations may be possible (see also Neuhäuser 2000, Neuhäuser & Comerón 2000):

- X-ray emission in young brown dwarfs may be due to the primordial magnetic fields of their parental molecular cores. The magnetic field of the cloud is frozen in the brown dwarf, as in normal late-type stars, but it decays very fast. The decay time-scale is not known, but is believed to lie somewhere between a few years and a few million years.
- X-ray emission of young brown dwarfs could be due to interaction between the brown dwarf magnetic field (due to either its own dynamo activity or a primordial magnetic field) and a possible gas and/or dust disk around the brown dwarf. Such disks are typical in young pre-main sequence stars like T Tauri stars, and may also exist in young brown dwarfs. There is some evidence for such disks in some of the young bona-fide and candidate brown dwarfs in ρ Oph (Wilking et al. 1999) as well as in some of the candidate brown dwarfs in Taurus (Briceño et al. 1998). Also, the X-ray detected bona-fide brown dwarf Cha Hα 1 shows excess emission in the ISO data (Comerón et al. 1999b; see Section 3.5).

If X-ray emission of brown dwarfs is due to dynamo activity, one would possibly expect a correlation between X-ray emission and rotation as in late-type stars. However, if X-ray emission of brown dwarfs is present only in very young objects, older brown dwarfs may very well rotate fast (eg. because they cannot loose a lot of angular momentum because of very weak winds), but at the same time show neither X-ray nor Hα emission. An example of a very late-type star with fast rotation, but neither X-ray nor Hα emission, is BRI0021$-$0214, with spectral type M9.5 (Basri et al. 1996; Neuhäuser 1999). However, this object is a star, not a brown dwarf, so that it still burns hydrogen in its center. However, the upper limit to its X-ray emission, $\log L_{\rm X}({\rm erg\ s}^{-1}) \leq 25.41$ (Neuhäuser 1999) corresponds to $log(L_{\rm X}/L_{\rm bol}) \leq -4.68$, which is slightly below the typical values found for X-ray detected very late-type stars. Hence, it may still be a very faint X-ray source.

If X-ray emission in these very late-type objects is thermal emission of hot plasma confined in magnetic fields, there should also be other magnetic activity like radio emission. Krishnamurthi et al.1999 have tried to detect radio emission from X-ray detected bona-fide and candidate brown dwarfs, selected from NC and Neuhäuser 1999, but they could not detect any object. Wilking et al. 1999 and Neuhäuser 1999 quote P. André (private communication) for the radio detection of the brown dwarf candidate GY 31 in the ρ Oph star forming region, identified as such by Wilking et al. 1999. This object was once detected at 3.6 cm with a flux of 0.5 mJy and once undetected with an upper limit of $\leq$ 0.1 mJy (P. André, private communication). This particular object has not been detected as X-ray source (Neuhäuser 1999) despite of very deep ROSAT PSPC and HRI pointings. The upper limit to the X-ray luminosity is $\log L_{\rm X}({\rm erg\ s}^{-1}) \leq 27.63$ and corresponds to $\log(L_{\rm X}/L_{\rm bol}) \leq -5.81$. Obviously, the radio and X-ray observations were not performed simultaneously.

Moreover, Neuhäuser 2000 and Neuhäuser & Comerón 2000 have searched the VLA Sky Survey source catalog (Condon et al. 1998) for radio emission of any of the known bona-fide and candidate brown dwarfs including the 2MASS objects. One object is detected as a radio source, namely the brown dwarf 2MASSWJ0438352+173634, a young Li-rich brown dwarf located behind the Hyades, probably in the Taurus star forming region (Gizis et al. 1999). This is the first radio detected brown dwarf. Its flux

Table 6. ISOCAM photometry or upper limits for the 13 faint late-type Chamaeleon I members.

ID	ISO[a]	$F_{6.7}$ mJy	$F_{14.3}$ mJy
1	95	6.7(1.8)	11.8(1.5)
2	111	24.5(1.4)	23.4(1.2)
3	116	5.9(0.9)	
4	-	<4.5	
5	144	7.4(1.3)	
6	152	12.7(1.5)	
7	-	<5.3	
8	-	<6.9	
9	98	11.4(0.9)	9.2(1.3)
10	-	<4.5	
11	-	<4.5	
12	-	<6.1	
13	137	8.0(0.8)	

[a] ISO-Cha I identification in Persi et al. (2000)

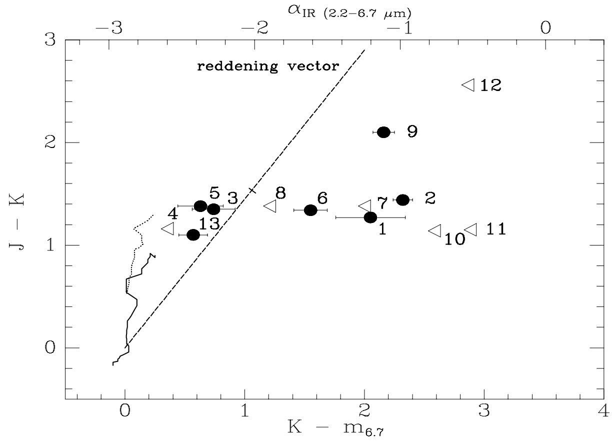

Fig. 7. The $(J-K), (K-m_{6.7})$ colour diagram for those of Cha Hα 1-13 detected by ISOCAM (filled circles) and ISOCAM upper limits (triangles). The solid line shows the reddening vector for an A0 star, adopting the Rieke & Lebofsky (1985) extinction law, and 10 magnitudes of visual extinction for an A0 star is indicated. Intrinsic colours of main sequence and giant stars are roughly indicated, based on Wainscoat et al. (1992). Individual error bars are given for the $K-m_{6.7}$ index. The near-IR fluxes are accurate to about 0.05 magnitudes (CRN).

at 1.4 GHz is 3.6±0.5 mJy, and the radio source is located 3″ off the 2MASS position. This particular object has not been included in any ROSAT pointed observation, so no meaningful measurements or upper limits on its possible X-ray emission exist as yet.

If it can be confirmed that young brown dwarfs usually are radio sources, or at least that X-ray emitting brown dwarfs usually are radio sources, then the following interpretation is supported, as in late-type stars: both X-ray and radio emission are due to magnetic activity, the X-ray emission being thermal emission from hot plasma confined in loops along the magnetic field lines and the radio emission being non-thermal gyro-synchroton emission from electrons gyrating around these magnetic field lines (see Neuhäuser 2000).

3.5. Results on thermal infrared emission.

As a general result of the ISOCAM star formation survey in several nearby molecular clouds, a large number of new Young Stellar Objects (YSOs) have been found through their mid-IR excesses (e.g. Nordh et al. 1996; Bontemps et al. 1998; Olofsson et al. 1999; Kaas et al. 2000). The excess sources are well separated from reddened field stars at mid-IR wavelengths, and intrinsic excess can safely be established from one single colour index. The mid-IR excess is likely to be due to thermal emission from dust in a circumstellar disk. The ISOCAM photometry (Persi et al. 2000) for the detected Cha Hα objects is shown in Table 6. For non-detections we have estimated upper flux limits case by case, due to noise and sky variations across the images from the presence of very bright sources and strong memory effects.

The 3 sources that are detected in both ISOCAM bands (Cha Hα 1, 2, and 9) all have excess emission in their $\log(F_{14.3}/F_{6.7})$ colour index. These are, together with the 4 sources with detections only at 6.7 μm, as well as those with only upper limits, plotted in a $(J-K), (K-m_{6.7})$ colour-colour diagram in Fig. 7. J and K magnitudes are taken from Table 1, and for Cha Hα 8, 12, and 13 we have used the J and K_s fluxes from the DENIS survey (Persi et al. 2000; Persi, priv comm). The extinction vector (Rieke & Lebofsky 1985) is indicated for an A0 star. The intrinsic colours of main-sequence and giant stars are taken from Wainscoat et al. (1992), and for the 6.7 μm band we have found approximate values by interpolating between 2.2 and 12 μm. From its location well to the right of the reddening vector, it is evident that also Cha Hα 6 has mid-IR excess. None or only negligible IR excess is found for sources Cha Hα 3, 4, 5, and 13, while nothing can be concluded about Cha Hα 7, 8, 10, 11 and 12.

Since all the Hα objects are found to be only modestly extinguished by the cloud ($A_V < 2$ magnitudes for all, see Table 4), the $K-m_{6.7}$ colour index is not contaminated by reddening, and therefore it is a reliable measurement of the intrinsic IR excess. According to the current picture of star formation and young stellar evolution (Adams et al. 1987; Lada 1987), YSOs can be classified according to the shape of their Spectral Energy Distributions (SEDs) as Class I (protostars), Class II (T Tauri stars) or Class III sources in an evolutionary sequence towards the main-sequence phase. In the absence of complete SEDs, which demand a huge observational effort, one can parametrize the SED by the mid-IR index $\alpha = d\log(\lambda F_\lambda)/(d\log\lambda)$, calculated between two wavelengths, usually from 2 μm to 10 or 20 μm. The mid-IR spectral index gives an indication of the amount of circumstellar dust and is a convenient tool in the IR spectral classification of YSOs. Sources with $-1.6 < \alpha < -0.3$ fall in the Class II group, according to the updated classification scheme (André & Montmerle 1994, Greene et al.1994). Here we have calculated an α between the two wavelengths 2.2 and 6.7 μm and found that $\alpha = -1.6$ corresponds to $K - m_{6.7} = 1.5$, and $\alpha = -0.3$ to $K - m_{6.7} = 3.1$. Sources in Fig. 7 which have $K - m_{6.7} > 1.5$ can therefore reliably be classified as Class II sources. Class IIs are characterized by having their circumstellar matter distributed in an optically thick disk. Most Classical T Tauri stars (CTTS) are Class II objects. For reference, the median intrinsic $J - K$ colour of CTTS in Taurus-Auriga is about 1.45 (Strom et al. 1993). Thus, we find clear signatures of circumstellar disks for 4 of the 13 low mass objects of this study, including the bona-fide brown dwarf Cha Hα 1.

The fact that some of these very low-mass objects are Class II sources would statistically imply ages of the order of 10^6 yrs. This is in nice agreement with the ages found from fitting the effective temperature and bolometric luminosities to the evolutionary models by Burrows et al. (1997) and Baraffe et al. (1998) (see Section 4 and Table 7) for 3 of the 4 Class II type objects. Only Cha Hα 9 is found to be somewhat older (20 - 25 Myr). The sources for which we find no IR-excess are, however, equally young according to this analysis. If all these objects were born with disks, the absence of a correlation between the derived age and the amount of IR-excess supports the idea of a wide range of variation in the disk dispersal timescale for different individual objects, allowing the coexistence of "old" objects like Cha Hα 9 still with a considerable infrared excess and "young" objects that show no trace of circumstellar material at the wavelengths studied here.

While no near-IR excess has been found for any of the 13 Hα emission line objects, *mid-IR* excesses are found for at least 4 of them. Fig. 8 shows the equivalent width of the Hα emission versus the mid-IR excess. It is clear that objects without mid-IR excess always have small equivalent widths (< 15 Å), while mid-IR excess objects can be found with any quantity of Hα emission. This is in good agreement with what is found for YSOs in general, e.g. by Kenyon & Hartmann (1995) who used $K - L$ as a measure of IR excess in Taurus-Auriga.

The lack of near-IR excesses for all these 13 Hα emission objects is somewhat surprising in view of the correlation commonly found between near-IR excess and strong Hα emission. It is well known, however, from studies of CTTS locations in the $(J-H), (H-K)$ colour-colour diagram (Lada & Adams 1992; Meyer et al. 1997), that many CTTS lack detectable near-IR excesses; up to 40% of them in Taurus-Auriga, according to Strom et al. (1993). In addition, we know from the ISOCAM surveys that the fraction of mid-IR excess sources which also exhibit detectable near-IR excesses, can be rather low. In the Serpens Cloud

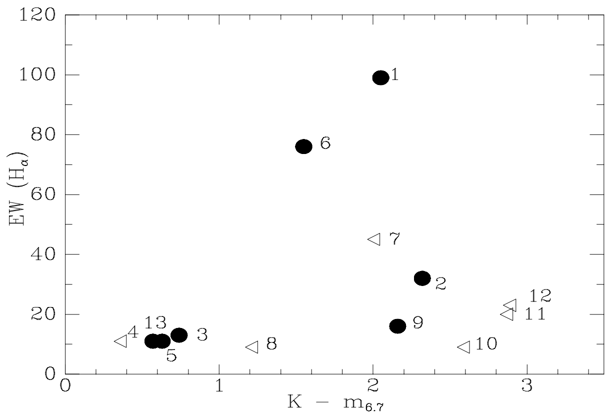

Fig. 8. Equivalent width of Hα emission versus mid-IR excess. Symbols as in Fig. 7. Note that triangles again are upper limits only for the $K - m_{6.7}$ colour.

Core this fraction is only ~ 0.5 (Kaas et al. 2000), while in Chamaeleon I as a whole, around 0.65 (Kaas 1999). For weak-lined T Tauri stars (WTTS), one usually attributes the presence of mid-IR excess and lack of near-IR excess to an inner hole in the circumstellar disk (e.g. Moneti et al. 1999). Sources which emit strongly in Hα, however, are believed to have inner disks since Hα emission usually is interpreted as a signature of the accretion process onto the surface of the object. But the near-IR wavelength region is strongly dominated by the photospheric emission, and rather large amounts of dust hot enough to produce a strong excess at 2 μm are therefore needed in order to distinguish intrinsic IR excess from the effects of scattering and extinction in the $(J - H), (H - K)$ diagram. A trend may thus be expected towards a decreasing fraction of objects with K band excess as one proceeds towards less massive objects, with lower temperatures and luminosities.

In Fig. 9 we show the $(J - H), (H - K)$ diagram for a number of ISOCAM Chamaeleon I sources with Hα equivalent widths ≥ 15 Å (open circles). The JHK photometry for these sources is taken from Prusti et al. (1992) and the Hα information from Hartigan (1993). Intrinsic colours of main-sequence, giant and supergiant stars (Koornneef 1982) are shown as bold curves, and the reddening line of an A0 star using an extinction law with slope $E(J - H)/E(H - K) = 1.7$ is shown as a dashed line. While 83% of these sources (open circles) have excess emission in the mid-IR, only about half of them are located sufficiently to the right of the reddening line to possess any near-IR excesses. The asterisks show the location of the 10 of the 13 very low mass stars and brown dwarf candidates of this study that have JHK photometry. The size of both types of symbols correlate with the 6.7 μm brightness (or in case of the faintest asterisks: the 6.7 μm upper limits). The flux in the 6.7 μm band is generally found to be proportional to the stellar luminosity

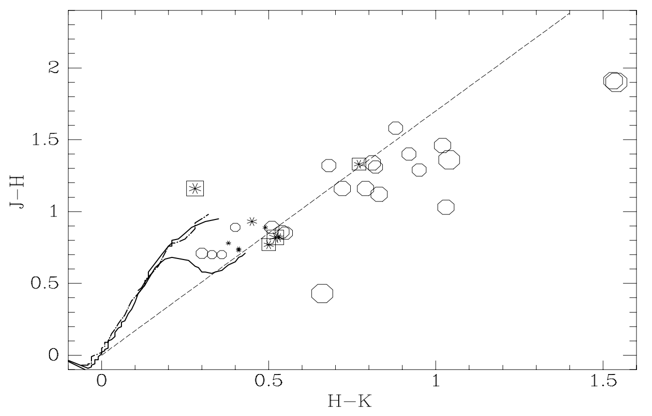

Fig. 9. The $(J-H),(H-K)$ colour diagram of all sources in the ISOCAM sample that have measured Hα emission equivalent widths $\geq$ 15 Å(open circles), together with the 10 of the 13 faint Hα sources of this study that have JHK photometry (asterisks). The symbol size is proportional to the 6.7 μm brightness; the smallest asterisks mean 6.7 μm upper limits. The 4 squares show the brown dwarf candidates with mid-IR excesses. Note that there are two nearly-overlapping points near $(J-H)=0.75$, $(H-K)=0.41$.

for YSOs. For Cha I the scatter is within a factor of $\sim$ 3 for IR excess sources and somewhat larger when including sources without IR excesses (see Persi et al. 2000). Such a correlation is expected for Class II type of YSOs if the 6.7 μm excess emission is dominated by reradiation of stellar light from a passive circumstellar disk (adding scatter due to different disk inclination angles) and not by the accretion luminosity from an active accretion disk, which is a reasonable interpretation in view of the recent findings of very low disk accretion rates for CTTS in general (Gullbring et al. 1998). In the following we thus use the 6.7 μm brightness as a rough indication of the stellar luminosity. It is then evident from Fig. 9 that the fainter sources are all located to the left of the dashed line, while the brightest ones are located to the right. Intermediate sources form a transitional group found on both sides.[3]. Hence, although our sample is small, we find a tendency for the presence of near-IR excesses in sources with strong Hα emission to be correlated with luminosity. This suggests that young stars with strong Hα emission and mid-IR excess, which are also expected to exhibit near-IR excesses, do so only if they are hot and luminous enough to arise sufficient temperature at the inner parts of the circumstellar disks, in agreement with model predictions of their emitted SED (Meyer et al. 1997).

[3] The only slight exception is Cha Hα 2, the leftmost object in the diagram. We note that this location could indicate the presence of scattered light in J and H, although extended emission is not detected in recent SOFI images in those bands having a full-width half maximum of 0"9.

4. The low-mass stellar and substellar population in Chamaeleon I

4.1. Physical properties

The accurate spectral types available for nearly all the stars of our sample allows their precise positioning in the temperature-luminosity diagram based on the availability of a reliable calibration of the temperature and the bolometric correction as a function of spectral type. The positions in the H-R diagram can in turn be compared to evolutionary model predictions, thus yielding estimates of the ages and masses of the objects.

The temperature scale that we have used is the one intermediate between dwarfs and giants proposed by Luhman 1999, which is $\simeq$ 150 K hotter than the one for dwarfs proposed by Leggett et al. 1996 and used by CRN over the range of spectral types of interest here. For an object of a given spectral type, the shift in the T_{eff} - L diagram implied by this new temperature scale results in a mass and an age that are respectively higher and older than those given by CRN using the dwarf temperature scale and the same set of evolutionary models. We note that this temperature scale has upper and lower bounds at any given spectral type set by the temperature scales of field M dwarfs and giants, respectively. As discussed by Luhman 1999, the former have been derived by Leggett et al. 1996 by fitting the observed spectral features to synthetic spectra at different temperatures, and are supported by measurements of the eclipsing binaries YY Gem and CM Dra (Luhman & Rieke 1998). On the other hand, the temperature scale for giants is obtained from measurements of stellar angular diameters. The scale proposed by Luhman 1999 is to some extent an *ad hoc* averaging between both scales that is validated, when combining it with the evolutionary tracks of Baraffe et al. 1998, by its satisfactory reproduction of the coevality of the four components of the GG Tau system (White et al. 1999) and the independence of the age with the mass in the H-R diagram of IC 348. Therefore, in a strict sense this temperature scale is consistent only when used in combination with the Baraffe et al. 1998 tracks (see below). However, given that it is a reasonable averaging of two temperature scales calibrated with independence of any evolutionary tracks, we will use the Luhman's 1999 scale as a convenient temperature vs. spectral type calibration, regardless of the actual set of pre-main sequence tracks used. An upper limit to the error introduced in this way is the largest difference between this calibration and the temperature of a dwarf or a giant of the same spectral type, namely about 200 K at spectral type M7, under the extreme assumption that the temperature scale of very young objects follows exactly either the field dwarf or the giant temperature scale. The actual uncertainty in the calibration is likely to be considerably smaller.

For late M dwarfs, the bolometric correction in the I_C band, BC_I, is small and changes relatively slowly with

Table 7. Adopted I_C-band bolometric corrections

spectral type	BC_I
M6	-0.28
M6.5	-0.35
M7	-0.43
M7.5	-0.51
M8	-0.59

spectral type (Kenyon & Hartmann 1995). However, surface gravity effects may be important, as can be seen by comparing the values of BC_I for dwarfs (Kenyon & Hartmann 1995) and giants (Fluks 1998), either at a given spectral type or at a given $(R_C-I_C)_0$ colour. For example, $BC_I = -0.05$ for a M6 dwarf, but it reaches -0.59 for a giant of the same spectral type; and if we compare the M6 dwarf to a M8 giant, which has the same $(R_C-I_C)_0$ colour, the value of BC_I for the latter reaches -1.6 mag. To account in an approximate way for systematic effects due to the surface gravity, we have used the BC_I vs. $(R_C-I_C)_0$ relationships for dwarfs and giants using the empirically determined values found in Kenyon & Hartmann 1995 and Fluks 1998 respectively, and have used them to fit the coefficients a_i of the function

$$BC_I = a_1 + a_2(R_C-I_C)_0 + a_3\log g + a_4(R_C-I_C)_0\log g \quad (4)$$

obtaining the values $a_1 = 2.757$, $a_2 = -1.838$, $a_3 = -0.335$, $a_4 = 0.270$. Assuming that $\log g = 4.9$, $\log g = 0.0$, and $\log g = 3.9$ are representative values for field M dwarfs, red giants, and very young objects at the age of Chamaeleon I respectively, we obtain for the latter:

$$BC_I = 1.451 - 0.785(R_C-I_C)_0 \quad (5)$$

The values of BC_I for the spectral types of interest here, derived through the adopted intrinsic colours listed in Table 3, are given in Table 7. At $(R_C-I_C)_0 = 2.30$ (M6.5 for very young objects), the difference between the BC_I so calculated and that of dwarfs is -0.3 mag, while the difference between giants and dwarfs at the same $(R_C-I_C)_0$ is -1.55 mag, i.e., our adopted BC_I are dwarf-like rather than giant-like, as would be expected from the closer spectral similarity of our objects with the former. As an external comparison, we have also calculated the coefficients a_i for the BC_I vs. $(R_C-I_C)_0$ relationship obtained from model atmospheres of dwarfs and giants by Lejeune et al. 1999, and have obtained an alternative BC_I scale which differs from ours by 0.24 mag at $(R_C-I_C)_0 = 2.30$ and 0.46 mag at $(R_C-I_C)_0 = 2.60$ (the reddest intrinsic colour assumed for our objects), in the sense of Lejeune et al's values being more negative than ours. Since Lejeune et al.'s models predict $BC_I \simeq -0.45$ for dwarfs with $(R_C-I_C)_0 = 2.30$, we believe that there are systematic effects in Lejeune's et al. scale which at least partially account as well for the differences between their BC_I scale and ours for young objects. It is difficult to give precise constraints on the systematic errors that may be present in the proposed BC_I vs. $(R_C-I_C)_0$ relationship, but assuming as a limiting hypothesis that the values of BC_I for very young objects may be actually identical to those of their field counterparts, we would be introducing an error of ~ 0.3 mag in BC_I.

Luminosities are calculated as

$$\log L(\mathrm{L}_\odot) = 1.86 - 0.4(I_C - A_I - DM + BC_I) \quad (6)$$

for which we have used the extinctions A_I listed in Table 4, and a distance modulus $DM = 6.0$ corresponding to the distance of 160 pc given in the Introduction.

The temperature-luminosity diagram for our objects is displayed in Figure 10. Comparisons are made to the temperature and luminosities predicted as a function of age and mass by two sets of evolutionary tracks, by Baraffe et al. 1998 and by Burrows et al. 1997. The individual ages and masses are given in Table 8.

A comparison of the results given in Table 8 shows that there is little variation in the estimated mass when using either Burrows et al. 1997 or Baraffe et al.'s 1998 evolutionary tracks. Incidentally, the same conclusion about the similarity of derived masses when using different evolutionary models was reached by CRN when comparing the evolutionary tracks of Burrows et al. 1997 and D'Antona & Mazzitelli 1997. Based on these results we can say that, if we accept the adopted spectral type vs. temperature calibration, our sample can be divided into three broad categories regardless of the pre-main sequence evolutionary tracks adopted. The first group, formed by Cha Hα 1, 7, 10, and 11 (M7.5-M8) consists of bona-fide brown dwarfs with masses around or below 0.05 $\mathrm{M}_\odot$. The second and most numerous group, Cha Hα 2, 3, 6, 8, 9, and 12 (M6.5-M7), is formed by transition objects near the borderline separating stars from brown dwarfs, and their true character cannot be decided unambiguously with the presently available data. Note that Neuhäuser & Comerón 1999 considered Cha Hα 3, 6 as bona-fide brown dwarfs on the basis of their M7 spectral type and lithium absorption. However, given their positions in the temperature-luminosity diagram from the revised calibrations used here and the uncertainties involved, it seems appropriate to adopt a more conservative borderline between stars and brown dwarfs, placing it at spectral type M7.5 instead. Finally, three objects of our sample, Cha Hα 4, 5, and 13 (M5-M6) are very probably very low mass stars.

Significant differences appear when considering the individual ages that we derive, both when comparing the present results with those of CRN, and when comparing the results that we obtain with each of the two sets of evolutionary tracks considered here. As we anticipated at the beginning of this Section, the adoption of a new

Table 8. Physical properties of very low-mass Chamaeleon I members, according to the adopted calibrations for the temperature and bolometric correction, and to the evolutionary models of Burrows et al. 1997 and Baraffe et al. 1998

			Burrows et al. 1997		Baraffe et al. 1998	
Object	T_{eff} (K)	log L($L_\odot$)	age (Myr)	mass ($M_\odot$)	age (Myr)	mass ($M_\odot$)
Cha Hα 1	2770	-1.96	8	0.05	2	0.04
Cha Hα 2	2910	-1.47	4.5	0.08	2	0.07
Cha Hα 3	2840	-1.46	2	0.07	< 2	0.06
Cha Hα 4	2980	-1.25	3.5	0.11	2	0.1
Cha Hα 5	2980	-1.31	3.5	0.11	2	0.1
Cha Hα 6	2840	-1.57	4	0.07	< 2	0.05
Cha Hα 7	2690	-2.19	10	0.05	2	0.03
Cha Hα 8	2910	-1.65	5.5	0.08	3	0.07
Cha Hα 9	2980	-2.26	25	0.09	20	0.07
Cha Hα 10	2770	-2.28	13	0.05	7	0.04
Cha Hα 11	2690	-2.44	15	0.04	10	0.03
Cha Hα 12	2840	-1.60	4.5	0.06	< 2	0.05
Cha Hα 13	3130	-0.97	3	0.2	2	0.2

temperature scale in the present work leads us to assign somewhat higher masses than those found in CRN. However, a more important effect of the new temperature scale comes from the fact that the new positions of the objects in the temperature- luminosity diagram place most of them past the deuterium-burning main sequence when using the tracks of Burrows et al., rather than near or before it as was the case in CRN. Likewise, the relative shift between the two sets of tracks considered here suffices to place many of our post-deuterium burning objects according to Burrows et al. on or near the deuterium-burning main sequence in Baraffe et al.'s models. For objects at the stellar/substellar boundary, the deuterium-burning phase lasts for about 3×10^6 years, extending to $\sim 8 \times 10^6$ years for the lowest masses found in our sample. This introduces differences of at least that amount in the derived age depending on whether an object is above or below the deuterium-burning main sequence. Unfortunately, the uncertainties in the position of objects in the temperature-luminosity diagram precludes a definitive conclusion on their evolutionary stage concerning their passage through the deuterium-burning main sequence, with the consequent large uncertainty in the age. However, the existence of a fairly large number of low mass stars in the region with ages near 2×10^6 years (see Section 4.2) suggests that the least massive members may not have passed yet through the deuterium-burning main sequence, thus indirectly favouring the models of Baraffe et al.

4.1.1. Fits using predicted colours from evolutionary models

Presently available evolutionary tracks for very low mass objects offer in principle a different approach to the derivation of the age and mass of the objects under study. A concern in the approach that we have followed so far is the need to transform observable quantities, such as spectral type or magnitude, into the input quantities required to query the models, namely temperature and luminosity. In this way, uncertainties in the transformations between spectral types, colours, temperatures, and bolometric corrections add up to the uncertainties of the evolutionary models themselves.

The integration of accurate atmosphere models in the latest generations of evolutionary tracks has allowed them to yield direct predictions of absolute magnitudes in different photometric bands. This removes the need for the adoption of an external temperature scale as a function of the spectral type or for the use of bolometric corrections, since both are built in the models themselves. The model predictions thus made are not free from systematic effects stemming from remaining shortcomings in the atmosphere models used, but at least ensure that the models and their predictions on observable quantites are self-consistent. Baraffe et al. 1998 have produced such models and provided comparisons with colour-colour diagrams of different clusters, finding a good agreement between theory and observations in a number of test cases. We have explored this more direct approach on our Chamaeleon I data as well.

To do this, we have used the I_C, J, and K bands, which are expected to be relatively free from possible errors arising from uncertainties in the TiO line list and departures from the plane-parallel atmospheres assumed by the models (Leggett et al. 1998; I. Baraffe, private communication). In turn, as discussed in Section 3.3, we do not expect circumstellar emission to provide a major contribution to the flux in the K band in our objects. The choice of a given model with fixed age and mass yields the expected absolute magnitudes M_λ at each band, which are related to the observed magnitudes m_λ by

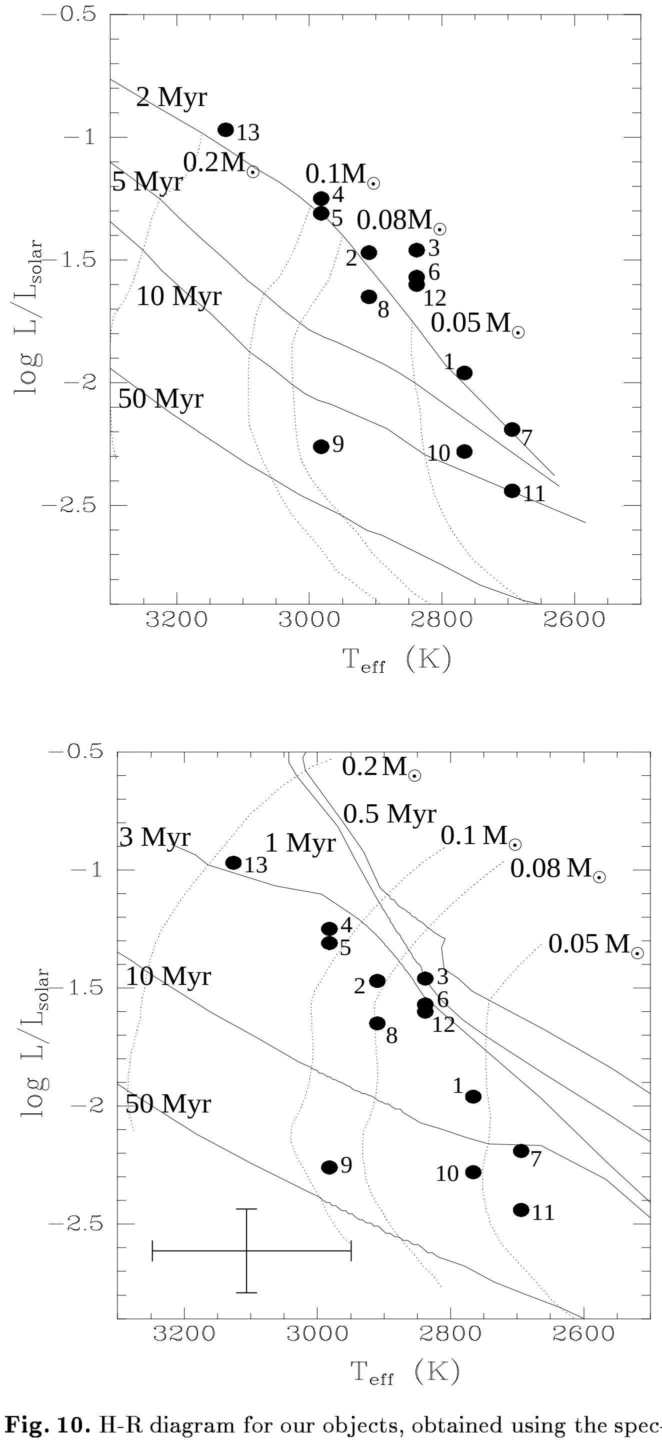

Fig. 10. H-R diagram for our objects, obtained using the spectral type vs. temperature calibrations and the bolometric corrections described in the text. The solid curves are isochrones, and dashed curves curves are lines of equal mass, based on Baraffe et al.'s 1998 models (upper panel) and on Burrows et al.'s models 1997 (lower panel). The error bars at the bottom left of the lower panel are conservative estimates of the uncertainties in temperature and luminosity near M7.The 150 K uncertainty in temperature includes the contribution of the accuracy in the spectral classification (assumed to be 0.5 spectral subclasses) and the dependence of the temperature vs. spectral type calibration on the surface gravity. The error in log L is dominated by the uncertainty in the BC_I as discussed in the text, to which we have added a contribution of a 0.2 mag uncertainty in the distance modulus.

$$M_\lambda = m_\lambda - \frac{A_\lambda}{A_V} A_V - DM \tag{7}$$

where the extinction A_V is the only adjustable parameter. A least-squares fit to the system of Eqs. (7) set by the different filters thus yields a best-fitting value of the extinction. By repeating the fit for a set of model objects within a range of masses and ages, we can take as an estimate of these quantities those that yield the lowest residual of the fit.

The results obtained in this way tend to yield higher masses, older ages, and higher temperatures for all the objects having I_C, J, and K photometry in our observations, and all of them require an extinction considerably higher than that listed in Table 4 in order to reproduce the observed colours. The substellar mass of the four latest objects in our sample, Cha Hα 1, 7, 10, and 11, is preserved in these fits, while the rest are best fit with masses typically between 0.1 and 0.2 M$_\odot$. In general, we find that the temperatures are too high for the spectral type vs. temperatures calibration discussed earlier by 150-300 K, exceeding the estimated uncertainty in the calibration.

A closer look at the strong correlation between the systematically higher temperatures that we obtain for the best fitting models and the higher extinction required to obtain a good fit clearly illustrates the main shortcoming of this method in which both temperatures (or intrinsic colours) and extinction are fit simultaneously. The basic problem is that in broad-band magnitude-colour-colour diagrams, the extinction vector forms a small angle with the the two-dimensional surface defined by the grid of models in the range of ages and masses in which we are interested. A consequence of this is the difficulty in isolating the effect of extinction: starting from a point in the plane defined by the models, it is necessary to move a long distance along the extinction vector in order to go to a point that is well separated from the surface defined by the models. As a practical consequence, if a low-temperature, low-extinction model yields a good fit to the measured magnitudes, it is usually possible to obtain an almost equally good fit with a higher-temperature, higher- extinction model. In this way, not only small systematic effects shifting the location of the models in the magnitude-colour- colour diagram, but also small variations in the extinction law and measurement errors in the photometry may lead to quite large disagreements between the best fitting temperature and luminosity of an object and the true values. We have checked that this is indeed the case for our fits by introducing random variations in the measured magnitudes, by arbitrarily reddening the model colours by only 0.2 magnitudes in I_C, and by assuming extinction laws with different total-to-selective extinction ratios as given in Steenman & Thé 1989. In general, redder colours of the models and higher total-to-selective extinction ratios in the extinction law tend to yield results closer to those of Table 7, but the correlation between both effects prevent us from quantifying each of them separately.

As a summary, despite the appealing properties of the use of predicted colours in removing the need for the adoption of external (and possibly inconsistent) calibrations, natural limitations arise from the characteristics of the extinction and the dependences of colours and magnitudes on mass and age at very low masses. These limitations make it necessary the use of complementary information such as the spectral type in order to constrain the intrinsic properties of the objects under study. However, we should mention that a promising way to deal with the problem described here maybe the use of narrow band filters allowing the definition of colour indices whose behaviour with mass and age could be clearly disentangled from the effects of extinction. Existing models that incorporate predicted atmospheric features can already provide useful guidance in the choice of the most appropriate filters.

4.2. Implications on the initial mass function and the star formation history

The presently available sample of 18 low mass members identified in the central area of the Chamaeleon I dark cloud raises two important questions concerning the statistics of its very low mass population: how complete is the present census of members in the surveyed area? And, what information do they provide concerning the initial mass function and the star formation history of the aggregate?

We can assess the completeness of the sample using the statistics on the expected number of sources per magnitude interval based on the K band star counts of CRN. In that paper, the expected distribution of apparent K magnitudes of background sources based on the Wainscoat et al. 1992 model was fitted to the faintest magnitude bins of the actual magnitude distribution, where the fraction of members of the star forming region is expected to be insignificant for any reasonable slope of the mass function. By extrapolating the expected distribution of background stars to the brightest bins, where the ratio of members to background sources is expected to increase, CRN showed that it is possible to statistically estimate the number of members of the aggregate, which will appear as an excess over the number of sources that would be expected if the only contribution were the background population. In this way, it is possible to constrain the slope of the mass function of the aggregate even if it is not possible to identify the members individually. The assessment of the completeness of our sample follows from the comparison between the number of expected members down to a certain magnitude, and the number of actually detected members.

This comparison is synthesized in Figure 11, which is an adaptation of Figure 5 of CRN. In it, the excess of sources over the extrapolated background down to a given

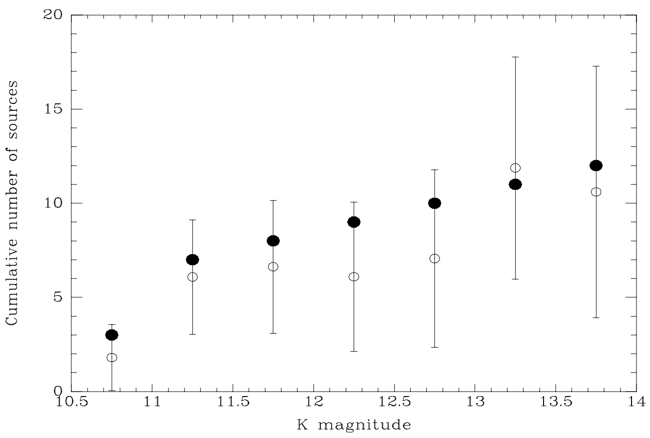

Fig. 11. Comparison between the estimated number of Chamaeleon I members as a function of K magnitude in the near-infrared survey of CRN (open circles), and the actual number of members identified by their Hα emission (filled squares). Only members fainter than $K = 10.5$ are considered. Error bars centered are $\sqrt{N}$ statistical uncertainties in the estimated numbers of sources.

K magnitude (together with its $\sqrt{N}$-uncertainty bars; see explanation in CRN) is compared to the actual number of identified members. Only objects fainter than $K = 10.5$, the saturation limit of CRN, are considered. Included in this plot are only those objects imaged in the near-infrared survey of CRN; three objects discussed in the present paper (Cha Hα 8, 12, and 13) are outside its boundaries and are therefore not considered in the comparison. On the other hand, we also include CHXR 73 and B34, two faint members that had been identified in previous surveys. As can be seen in Figure 11, there is no evidence for any significant fraction of as yet unidentified members of the aggregate in the area of the near-infrared survey, suggesting that the completeness of our sample is close to unity. Since all the members considered here have been identified due to their Hα emission, our results indicate that samples of low mass stars selected on the basis of this feature are highly complete at the age of the Chamaeleon I population (although the same is not true for populations whose ages exceed 10^7 years; see e.g. Briceño et al. 1999). This seems to be in contrast with the results of Luhman et al. 1998 and Herbig 1998, who obtained completeness fractions of $\sim$ 40% in IC 348, a cluster with age probably similar to that of Chamaeleon I. We note however that their equivalent width detection limit, 10 Å, is very close to the equivalent width that we measure for about half of our sources, which in turn is highly variable (see Table 1, and compare to Table 4 of CRN, and to Table 1 of Neuhäuser & Comerón 1999). The incompleteness of Hα-selected samples may thus be related to the fact that many of the low mass members may have Hα emission near the detection limit, suggesting that more sensitive surveys like ours should be able to produce complete, or nearly complete, samples. The more recent detection of additional members of IC 348 with Hα equivalenth widths below 10 Å reported by Luhman 1999 lends support to our suggestion.

An interesting additional check on the completeness of the Hα-selected sample can be made by comparing the objects found in this way to the objects independently selected by means of their mid-IR emission detected by ISOCAM. Three of the new Chamaeleon I members identified in ISOCAM observations by Persi et al. 2000 (numbers 68, 71, and 79 in their Table 2) are not present in our Hα sample, despite of their location within the boundaries of our survey. A closer inspection of their published JK_s magnitudes shows that the $(J-K_s)$ of objects 71 and 79 is respectively 0.76 and 1.02 magnitudes redder than that of the reddest object in our sample, Cha Hα 9 (whose $(J-K)=2.10$ is in turn largely attributed to extinction). Moreover, these two objects lie to the West of the ones in our Hα sample, in a region where visible-light images clearly show a strong extinction on the background. We thus attribute their redder color to the fact of them being more embedded in the cloud than the Hα detected objects, and therefore heavily obscured in the Hα region. As to object 68 in Persi et al. 2000, we find that the $J-K_s$ of the tentative near-infrared counterpart is in this case bluer than the bluest objects in our Hα sample. Moreover, we note that this object is flagged as an uncertain near-infrared identification by Persi et al. and that, like the other two, it lies in a region of high background extinction. Taken together, this leads us to believe that the assumed near-infrared identification may be erroneous, as hinted by Persi et al., and that the true counterpart of this object is actually a heavily reddened source too faint to be detected by the DENIS survey on which the near-infrared identifications of Persi et al. are based. Unfortunately, although our near-infrared survey reaches to fainter magnitudes than DENIS, object 68 lies just outside its area of coverage and we cannot provide an alternative identification.

As a summary of the comparison between the mid-infrared and the Hα selected samples, we believe that the arguments given above concerning the essential completeness of the Hα selected sample are confirmed when considering objects with mid-infrared excess, given that no mid-IR selected member of the aggregate is bright enough in the Hα region and yet undetected in Hα emission. On the other hand, the existence of the these additional objects increases by two the number of identified members in the three rightmost bins of the cumulative distribution of Figure 11 (as noted above, the third object, number 68 in Persi et al. 2000, is out of the area covered in the infrared survey on which the starcounts statistics are based), still consistent with the statistical expectations from starcounts described by CRN.

The high degree of completeness that we estimate for our sample allows us to explore the initial mass function through the individual masses estimated for each object, rather than constraining it statistically as was done in CRN. The entire sample that we use for this purpose consists of the 13 Hα emitting sources reported in the present work and in CRN, plus 9 more massive objects previously detected in the same area covered by the Hα surveys presented here. These objects are HM 15, 19; CHXR 21, 22, 73, 74, 78C; Sz 23; and B 34. Six more more stars (LHα 332-17, VW Cha, HD 97048, Glass Ia, HM 16, and CHXR 26) appear to have masses larger than 1 $M_\odot$, the upper limit that we consider here. The same is probably true for the star exciting the Chamaeleon Infrared Nebula (Cohen & Schwartz 1984, Ageorges et al. 1996), which also appears in our survey as the intense fan-shaped nebulosity near the upper left corner of the bottom image in Figure 1. Spectral types have been taken from CRN for CHXR 73, CHXR 74, CHXR 78C, B34, HM 15, and Sz 23. Luminosities for these objects are taken directly from CRN, as the bolometric corrections adopted there do not differ significantly from an extrapolation of the ones used here for these early M stars. However, the temperatures for those objects that we use here have been revised according to the new scale of Luhman 1999. For HM 19 and CHXR 22, we have used the spectral types of Lawson et al. 1996, but also with the Luhman 1999 temperature scale. The luminosities assigned to these objects are those of Lawson et al. 1996. Finally, for CHXR 21, we have used both the temperature and the luminosity given by Lawson et al. 1996: given the excellent agreement between the temperatures used by Luhman 1999 and Lawson et al. 1996 at early M types, we believe that using Lawson et al.'s temperature for this K7 object does not introduce any significant inconsistency.

Figure 12 plots the temperature-luminosity diagram for all the stars and brown dwarfs identified in the surveyed area having masses below 1 $M_\odot$, with the isochrones and lines of equal mass of Baraffe et al. 1998 superimposed. Perhaps the most remarkable feature of this figure is the clustering of the majority of the objects towards the 2 Myr isochrone, apparent in the distribution of objects with masses below 0.5 $M_\odot$. The small scatter found in ages suggests an essentially coeval population having formed over a time span of less than one million years, in agreement with recent results found for other low mass star forming regions like ρ Ophiuchi and IC 348 (Luhman & Rieke 1999, Luhman 1998) as well as for regions where low and high mass star formation has proceeded simultaneously, such as the Scorpius-Centaurus OB association (Preibisch & Zinnecker 1999). The small scatter at all masses and the absence of any apparent trends correlating age and mass also support the validity of the adopted models and calibrations throughout the range of masses and temperatures sampled by these objects. However, the existence of a small number of objects with ages around $\sim 2\times10^7$ years (which, from hotter to cooler in Figure 12, are CHXR 21, Sz23, and Cha Hα 9) seems also well estab-

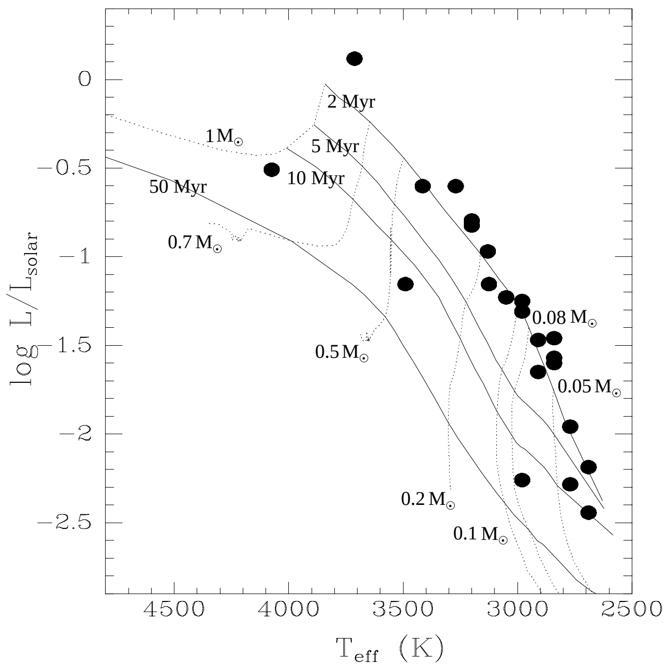

Fig. 12. Temperature-luminosity diagram with all members less massive than 1 M$_\odot$ identified in the region shown in Figure 1, with the evolutionary tracks of Baraffe et al. 1998 superimposed.

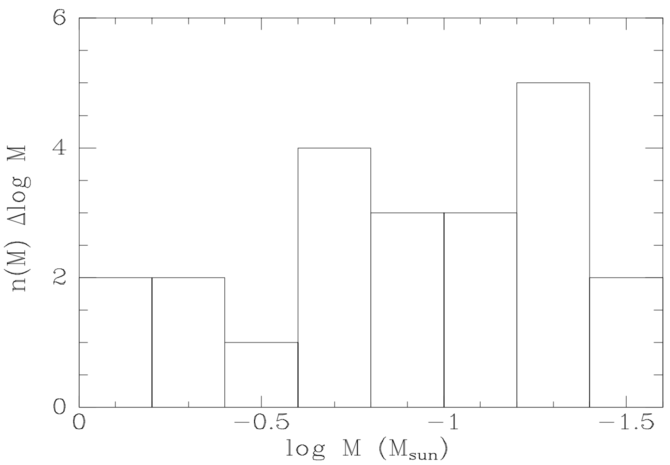

Fig. 13. The mass function as defined by the members of Chamaeleon I identified so far in the surveyed region and with masses below 1 M$_\odot$. The evolutionary tracks of Baraffe et al. 1998 have been used.

lished. Cha Hα 10 and 11 also seem to be somewhat older, but the increased slope of the isochrones at the lowest masses makes the estimated age highly dependent on the assigned temperature and their coevality with the more massive members cannot be entirely ruled out. The rough coevality of the three clearly deviant objects, and the lack of objects with masses between ~ 3 and ~ 20 Myr, might be indicative of two distinct bursts of star formation having taken place in the region. However, the larger sample studied by Lawson et al. 1996 shows that other areas of the cloud do possess members, some of them classical T Tauri stars, that lie in the gap between both isochrones in the temperature-luminosity diagram.

Figure 13 shows the histogram of masses in logarithmic mass intervals. Using one of the common approximations to the mass function,

$$n(M)\, d\log M \propto M^{-\alpha+1}\, d\log M \qquad (8)$$

we find $\alpha \sim 1.1$, corresponding to a mass function slowly rising towards the smaller masses in linear mass units, and nearly flat in logarithmic mass units, roughly compatible with findings both in nearby star forming regions and in the field. The small number of objects on which our statistics are based do not exclude neither the possibility of a mildly declining mass function below 0.4 M$_\odot$, as claimed by Luhman & Rieke 1999 for ρ Ophiuchi and maybe other clusters and star forming regions, nor a somewhat steeper slope as found by Reid et al. 1999 for the field ($\alpha = 1.3$).

5. Conclusions

The multiwavelength observations presented here have allowed us to carry out a comprehensive study of the lowest mass population of a small area at the center of the Chamaeleon I star forming region, addressing a variety of issues related to their intrinsic properties, their observational features, and their statistics. We have discussed the results of our visible and near infrared imaging, visible and near infrared low resolution spectroscopy, and space-based X-ray observations and thermal infrared imaging. Our main findings can be summarized as follows:

1- Seven new members with late M spectral types have been identified thanks to their Hα emission in an area of ~ 300 arcmin^2 at the center of the Chamaeleon I aggregate. Taking into account the results of previous works, this raises to 22 the number of members with masses below 1 M$\odot$ identified in the area. The spectral types of six of the newly identified members can be determined with accuracy thanks to high quality low resolution spectroscopy at visible wavelengths, and range from M6 to M8.

2- We have explored the correlation of different indices proposed by different authors with the spectral type as a way to obtain a quantitative spectral classification based on narrow-band photometry in the red. We find the VO index defined by Kirkpatrick et al. 1995 to be the one best correlated with spectral type. On the other hand, the ratio C defined by Kirkpatrick et al. 1991 which measures the strength of the gravity-sensitive NaI feature near 8190 Å is found to provide an excellent tool for the identification of young very low mass stars and brown dwarfs, allowing their discrimination both from more evolved field M dwarfs types and from M giants with similar spectral types.

3- We have produced representative spectra in the K band by combining those of the late M-type objects with similar classifications in the visible (less than half a subclass apart). We find no obvious correlation with the spectral type of any of the features identified at low resolution in the 2 μm region. This indicates that, at best, only a rather coarse classification is possible for very late M very young objects using low resolution K band spectra. No trends are clear either when using a reddening-free index based on the depth of the wings of the broad water vapour absorption band centered near 1.9 μm.

4- Seven of the objects with spectral types M6 or later display X-ray emission detected in deep ROSAT pointings, including one bona-fide brown dwarf and three objects near the transition between stars and brown dwarfs. Five other late-type objects, including three bona-fide brown dwarfs, are too close to bright X-ray emitting stars to enable unambiguous detection, and only one object with M6 spectral type is clearly undetected. The emission levels of our objects are in the range $-3.21 > L_x/L_{\rm bol} > 4.12$, similar to those of other young late-type, fully convective stars. The non-detection of older brown dwarfs in other clusters and in the field support the view that X-ray emission among brown dwarfs may be restricted to the earliest stages of evolution.

5- Seven of the 13 low mass objects are detected in an ISOCAM survey at 6.7 μm, and four of these have intrinsic mid-IR excesses typical of Class II young stellar objects (YSOs). Thus, circumstellar disks are found for one bona-fide brown dwarf and three objects near the transition between stars and brown dwarfs. The relation between the strength of the Hα emission and mid-IR excess is consistent with that of YSOs in general. From a larger ISOCAM sample in Chamaeleon I we find a slight tendency for the presence of near-IR excesses in Hα emission sources to be correlated with luminosity. This may suggest that the lack of near-IR excesses in the low mass objects is due to their incapability to arise sufficient temperature at the inner parts of the circumstellar disk to create a detectable K-band excess.

6- We use published pre-main sequence evolutionary models and temperature-spectral type calibrations, and propose bolometric corrections, that enable us to estimate ages and masses for our sample of objects later than M5. According to two different recent sets of models (Burrows et al. 1997 and Baraffe et al. 1998), four of these objects, having spectral types M7.5-M8, can be considered as bona-fide brown dwarfs. Six other objects, classified as M6.5-M7, have masses near the borderline separating very low mass stars from brown dwarfs, and their true nature cannot be decided with presently available models and calibrations. The other three objects, with spectral types M5-M6, are very likely low mass stars. The two sets of models used assign similar masses assigned to our objects, but have a larger disagreement on the assigned ages, in the sense of Burrows et al. yielding older ages. The cause of the discrepancy is due to the relative location of the objects with respect to the deuterium-burning main sequence. Arguments based on the population of the aggregate at somewhat higher masses suggest that Baraffe et al.'s models give ages closer to the actual value.

7- Using statistical arguments based on K-band star counts published in an earlier paper, we demonstrate that the Hα-selected sample of very low mass stars discussed here shows no evidence for significant incompleteness. This suggests that surveys sensitive to Hα equivalent widths below 10 Å in aggregates only a few million years old are an efficient probe of the faintest end of the stellar main sequence and the massive end of the brown dwarf population. Studies carried out by other authors seems to indicate however that this may not be the case for populations older than $\sim 10^7$ years.

8- The vast majority of identified members in the surveyed region with masses below 1 $M_\odot$ have ages near 2×10^6 years, with only three objects clearly having ages significantly older $\sim 2 \times 10^7$ years). This suggests that a short-lived burst of low mass star and brown dwarf formation took place in Chamaeleon I approximately 2×10^6 years ago, although star forming activity at a lower rate had been already taking place since perhaps 2×10^7 years before.

9- The mass function in the surveyed area of Chamaeleon I is consistent with the majority of published derivations of the mass function in star forming regions and in the field, being roughly flat in logarithmic mass units.

Acknowledgements. It is a pleasure to thank the NTT and 2p2 Teams in ESO-La Silla, especially Dr. Stephane Brillant at the NTT and Dr. Alessandro Pizzella at the 1.5 m Danish telescope, for excellent support. The efficient work of the telescope operators at the NTT during our April 1999 run, Mr. Ariel Sánchez and Mr. Hernán Núñez, greatly contributed to its success. We thank the astronomers in charge of the service observing at the NTT when our SOFI observations were performed, as well as the User Support Group at ESO-Garching for the careful review of the Observing Blocks submitted by us to ensure that the observations would be properly carried out. We thank Dr. Isabelle Baraffe for her very helpful remarks concerning the model predictions on broad band colours and for making available to us data prior to publication. Comments by the referee, Dr. J. R. Stauffer, helped to clarify many points in the paper.

References

Adams, F.C., Lada, C.J., Shu, F.H., 1987, ApJ 312, 788.
Ageorges, N., Fischer, O., Stecklum, B., Eckart, A., Henning, Th., 1996, ApJ, 463, L101.
André, P., Montmerle, T., 1994, ApJ, 420, 837.
Baraffe, I., Chabrier, G., Allard, F., Hauschildt, P.H., 1998, A&A, 337, 403.
Basri, G., Marcy, G., & Graham, J. 1996, ApJ, 458, 600.
Bontemps, S., Nordh, L., Olofsson, G., et al. 1998, In: Starformation with ISO, eds. Yun, J., Liseau, R., p. 141.
Briceño, C., Hartmann, L., Stauffer, J., Martín E. 1998, AJ, 115, 2074

Briceño, C., Calvet, N., Kenyon, S., Hartmann, L., 1999, ApJ, 118, 1354.

Burrows, A., Marley, M., Hubbard, W.B., Lunine, J.I., Guillot, T., Saumon, D., Freedman, R., Sudarsky, D., Sharp, C., 1997, ApJ, 491, 856.

Cambrésy, L., Epchtein, N., Copet, E., de Batz, B., Kimeswenger, S., Le Bertre, T., Rouan, D., Tiphène, D., 1997, A&A, 324, L5.

Cambrésy, L., 1999, A&A, 345, 965.

Cohen, M., Schwartz, R.D., 1984, AJ, 89, 277.

Comerón, F., Rieke, G.H., Neuhäuser, R., 1999a, A&A, 343, 477 (CRN).

Comerón, F., Neuhäuser, R., Kaas, A.A., 1999b, The Messenger, 94, 28.

Condon, J.J., et al., 1998, AJ 115, 1693 (VLA Sky Survey)

Crawford, D.L., Perry, C.L., 1976, AJ, 81, 419.

D'Antona, F., Mazzitelli, I., 1997, Mem. S. A. It. 68, 807.

Fluks, M.A., 1998, PhD Thesis, Univ. of Amsterdam.

Gauvin, L.S., Strom, K.M., 1992, ApJ, 385, 217.

Gizis, J.E., Reid, I.N., & Monet, D.G. 1999, AJ, 118, 997

Greene, T.P., Wilking, B.A., André, P., Young, E.T., Lada, C.J., 1994, ApJ, 434, 614.

Gullbring, E., Hartmann, L., Briceño, C., Calvet, N., 1998, ApJ, 492, 323.

Hartigan, P., 1993, AJ, 105, 1511.

Herbig, G.H., 1998, ApJ, 497, 736.

Hillenbrandt, L.A., 2000, in "From darkness to light: origin and evolution of young stellar clusters", eds. T. Montmerle and P. André, ASP Conf. Ser., in press.

Jones, H.R.A., Longmore, A.J., Jameson, R.F., Mountain, C.M., 1994, MNRAS, 267, 413.

Jones, H.R.A., Longmore, A.J., Allard, F., Hauschildt, P.H., 1996, MNRAS, 280, 77.

Kaas, A.A., 1999, PhD Thesis, Stockholm University.

Kaas, A.A., Olofsson, G., Bontemps, S. et al. 2000, in prep.

Kenyon, S.J., Hartmann, L., 1995, ApJS, 101, 117.

Kirkpatrick, J.D., Henry, T.J., McCarthy, D.W., 1991, ApJS, 77, 417.

Kirkpatrick, J.D., Henry, T.J., Simons, D.A., 1995, AJ, 109, 797.

Kirkpatrick, J.D., Reid, I.N., Liebert, J., Cutri, R.M., Nelson, B., Beichman, C.A., Dahn, C.C., Monet, D.G., Gizis, J.E., Skrutskie, M.F., 1999, ApJ, 519, 802.

Knude, J., Høg, E., 1998, A&A, 338, 897.

Koornneef, J., 1983, A&A, 128, 84.

Krishnamurthi, A., Leto, G., & Linsky, J.L. 1999, AJ, 118, 1369

Lada, C.J., 1987, In: IAU Symp. 115, Star Forming Regions, eds. Peimbert, M. & Jugaku, J., p.1.

Lada, C.J., Adams, F.C., 1992, ApJ 393, 278.

Lawson, W.A., Feigelson, E.D., Huenemoerder, D.P., 1996, MNRAS, 280, 1071.

Leggett, S.K., Allard, F., Berriman, G., Dahn, C.C., Hauschildt, P.H., 1996, ApJS, 104, 117.

Leggett, S.K., Allard, F., Hauschildt, P.H., 1998, ApJ, 508, 836.

Lejeune, T., Cuisinier, F., Buser, R., 1998, A&AS, 130, 65.

Luhman, K.L., 1999, ApJ, 525, 466.

Luhman, K.L., Rieke, G.H., 1998, ApJ, 497, 354.

Luhman, K.L., Rieke, G.H., 1999, ApJ, 525, 440.

Luhman, K.L., Liebert, J., Rieke, G.H., 1997, ApJ, 489, L165.

Martín, E.L., Rebolo, R., Zapatero-Osorio, M.R., 1996, ApJ, 469, 706.

Meyer, M.R., Calvet, N., Hillenbrand, L.A., 1997, AJ, 114, 288.

Meyer, M.R., Edwards, S., Hinkle, K.H., Strom, S.E., 1998, ApJ, 508, 397.

Moneti, A., Zinnecker, H., Brandner, W., Wilking, B., 1999, In: Astrophysics with Infrared Surveys: A Prelude to SIRTF, eds. Bicay, M.D., Cutri, R.M., Madore, B.F., ASP Conf. Ser. 177, p. 355.

Neuhäuser, R., 2000, "X-ray emission and coronal activity of brown dwarfs", in "Giant planets to cool stars", eds. C. Griffith & M. Marley, ASP Conf. Ser., in press.

Neuhäuser, R., Comerón, F., 1998, Science, 282, 83 (NC).

Neuhäuser, R., Comerón, F., 1999, A&A, 350, 612.

Neuhäuser, R., Comerón, F., 2000, "Coronal activity of brown dwarfs"', in "11th Cambridge Workshop on Cool Stars, Stellar Systems, and the Sun", ed. R. Rebolo, in press.

Neuhäuser, R., Sterzik M.F., Schmitt, J.H.M.M., Wichmann R., Krautter J., 1995, A&A, 297, 391.

Neuhäuser, R., Briceño, C., Comerón, F., Hearty, T., Martín, E.L., Schmitt, J.H.M.M., Stelzer, B., Supper, R., Voges, W., Zinnecker, H., 1999, A&A, 343, 883.

Nordh, L., Olofsson, G., Abergel, A., et al. 1996, A&A, 315, 185.

Oasa, Y., Tamura, M., Sugitani, K., 1999, ApJ, 526, 336.

Olofsson, G., Kaas, A.A., Nordh, L., et al. 1998, in "Brown Dwarfs and Extrasolar Planets", eds. R. Rebolo, E.L. Martin, M.R. Zapatero Osorio, ASP Conf. Ser. 134, p. 81.

Olofsson, G., Huldtgren, M., Kaas, A.A., et al. 1999, A&A 350, 883.

Persi, P., Marenzi, A.R., Olofsson, G., et al. 2000, A&A, in press.

Preibisch, Th., Zinnecker, H., 1999, AJ, 117, 2381.

Prosser, C.F., Stauffer, J., Kraft, R.P., 1991, AJ, 101, 1361.

Prusti, T., Whittet, D.C.B., Wesselius, P.R., 1992, MNRAS, 254, 361.

Reid, I.N., Kirkpatrick, J.D., Liebert, J., Burrows, A., Gizis, J.E., Burgasser, A., Dahn, C.C., Monet, D., Cutri, R., Beichman, C.A., Skrutskie, M., 1999, ApJ, 521, 613.

Rieke, G.H., Lebofsky, M.J., 1985, ApJ, 288, 618.

Schwartz, R.D., 1991, in "Low Mass Star Formation in Southern Molecular Clouds", Ed. B. Reipurth, ESO Sci. Rep. 11.

Shu, F.H., Adams, F.C., Lizano, S., 1987, ARA&A, 25, 23.

Steenman, H., Thé, P.S., 1989, Ap&SS, 159, 189.

Strom, K.M., Strom, S.E., Merrill, K.M., 1993, ApJ 412, 233.

Wainscoat, R.J., Cohen, M., Volk, K., Walker, H.J., Schwartz, D.E., 1992, ApJS, 83, 111.

White, R.J., Ghez, A.M., Reid, I.N., Schultz, G., 1999, ApJ, 520, 811.

Whittet, D.C.B., Kirrane, T.M., Kilkenny, D., Oates, A.P., Watson, F.G., King, D.J., 1987, MNRAS, 224, 497.

Wichmann, Bastian, U., Krautter, J., Jankovics, I., Rucinsky, S.M., 1998, MNRAS, 301, L39.

Wilking, B.A., Greene, T.P., Meyer, M.R., 1998, AJ, 117, 469.

Williams, D.M., Rieke, G.H., Stauffer, J.R., 1995, ApJ, 445, 359.

Zapatero Osorio, M.R., Martín, E.L., Rebolo, R., 1997, A&A, 323, 105.